PRODUCTION OF ALUMINA BOROSILICATE CERAMIC NANOFIBERS BY USING ELECTROSPINNING TECHNIQUE AND ITS CHARACTERIZATION

A THESIS SUBMITTED TO
THE GRADUATE SCHOOL OF NATURAL AND APPLIED SCIENCES
OF
MIDDLE EAST TECHNICAL UNIVERSITY

BY

SENEM TANRIVERDİ

IN PARTIAL FULFILLMENT OF THE REQUIREMENTS
FOR
THE DEGREE OF MASTER OF SCIENCE
IN
CHEMICAL ENGINEERING

JUNE 2006

Approval of the Graduate School of Natural and Applied Sciences

Prof. Dr. Canan Özgen
Director

I certify that this thesis satisfies all the requirements as a thesis for the degree of Master of Science.

Prof. Dr. Nurcan Baç
Head of Department

This is to certify that we have read this thesis and that in our opinion it is fully adequate, in scope and quality, as a thesis and for the degree of Master of Science.

Prof. Dr. Üner Çolak
Co-Supervisor

Prof. Dr. Güngör Gündüz
Supervisor

Examining Committee Members

Prof. Dr. Deniz Üner	(METU, CHE)
Prof. Dr. Güngör Gündüz	(METU, CHE)
Prof. Dr. Üner Çolak	(HU., NEM)
Assoc. Prof. Dr. Gürkan Karakaş	(METU, CHE)
Ph. D. Bora Maviş	(HU., IE)

I hereby declare that all information in this document has been obtained and presented in accordance with academic rules and ethical conduct. I also declare that, as required by these rules and conduct, I have fully cited and referenced all material and results that are not original to this work.

Name, Last name : Senem Tanrıverdi
Signature :

ABSTRACT

PRODUCTION OF ALUMINA BOROSILICATE CERAMIC NANOFIBERS USING ELECTROSPINNING TECHNIQUE AND ITS CHARACTERIZATION

Tanrıverdi, Senem
M.S., Department of Chemical Engineering
Supervisor: Güngör Gündüz, Prof. Dr.
Co-Supervisor: Üner Çolak, Prof. Dr.

June 2006, 71 pages

Today, ceramic, polymer, and composite nanofibers are among the most charming materials for nanotechnology. Because of their small characteristic dimension, high surface area, and microstructural features, they provide unique mechanical, optical, electronic, magnetic, and chemical properties for an extensive variety of materials applications.

Electrospinning provides an effective way of the nanofiber production in a nanometer scale. This technique utilizes a high voltage DC to create a strong electric field and a certain charge density in a viscous solution contained in a pipette. As a result, fibers with diameters ranging from the micrometer to nanometer are formed from this charged solution.

This study deals with, the fabrication of alumina borosilicate ceramic nanofibers using electrospinning technique. Alumina borosilicates contain important components having intriguing characteristics for many applications and have been widely studied with different compositions.

In this study, alumina borosilicate/PVA solution was prepared using the conventional sol-gel method. Polyvinyl alcohol (PVA) was added into this solution to increase the viscosity for electrospinning. After the alumina borosilicate/PVA solution was electrospun into fibers, high temperature sintering was carried to obtain ceramic alumina borosilicate fibers. The products were characterized by scanning electron microscopy (SEM), X-ray diffractometry (XRD), Fourier transform-infrared spectroscopy (FT-IR), and thermogravimetric/differential thermal analysis (TG-DTA) techniques.

Keywords: alumina borosilicate, ceramic nanofibers, sol-gel, electrospinning, nanotechnology.

ÖZ

ELEKTROSPİNLEME YÖNTEMİYLE ALUMİNA BOROSİLİKAT SERAMİK NANOELYAFLARIN ÜRETİMİ VE ÖZELLİKLERİNİN BELİRLENMESİ

Tanrıverdi, Senem
Yüksek Lisans, Kimya Mühendisliği Bölümü
Danışman: Güngör Gündüz, Prof. Dr.
Yardımcı Danışman: Üner Çolak, Prof. Dr.

Haziran 2006, 71 sayfa

Günümüzde seramik, polimer ve kompozit nanoelyaflar nanoteknolojinin en cazip ürünleri arasındadır. Boyutlarının küçük, yüzey alanının büyük olmasından dolayı, çeşitli uygulamalar için eşsiz mekanik, optik, elektronik, manyetik ve kimyasal özellikler sağlarlar.

Elektrospinleme tekniği, son zamanlarda nano boyutta elyaf üretimi için sıkça kullanılmaktadır. Elektrospinleme işleminde, içinde çözelti bulunan kapiler uca sahip bir hazne ile metalik malzemeden yapılmış ve fiberlerin toplanmasında kullanılan toplama yüzeyi arasında yüksek bir elektrik alan oluşturulur. Voltaj kritik bir seviyeye ulaşınca, kapiler ucunda askıda duran damlacık yüzeyinde oluşan yük, yüzey gerilimini yenerek bir jet oluşumuna neden olur. Elektriksel olarak yüklü jet, yarılarak ya da esneme hareketleriyle incelerek toplama yüzeyinde dağınık olarak toplanır.

Bu çalışmada, elektrospinleme yöntemiyle alumina borosilikat seramik nanoelyaf üretimi gerçekteştirilmiştir. Alumina borosilikatlar, yapısında birçok uygulama için ilgi çekici özelliklere sahip bileşenler içerir ve şu ana kadar, farklı bileşimlerde yapılmış çalışmaları yaygın olarak bilimsel kaynaklarda bulunmaktadır.

Elektrospinleme tekniği ile alumina borosilikat elyaf üretimi için gereken çözeltinin hazırlanmasında çöz-pel (sol-gel) yöntemi kullanılmıştır. Hazırlanan çözeltinin viskozitesini ayarlayabilmek için polivinil alkol (PVA) katılmış ve ardından çözelti spinlenmiştir.

Oluşan alumina borosilikat/PVA içerikli elyaflar yüksek sıcaklarda sinterlendikten sonra alumina borosilikat elyaflar elde edilmiştir. Taramalı elektron mikroskopu (SEM), X-ışını kırınımı (XRD), Fourier dönüşümlü kızılötesi spektrumu (FT-IR), termogravimetrik ve diferansiyel termal analiz (TG-DTA) teknikleri kulanılarak ürünün özellikleri belirlenmiştir..

Anahtar Sözcükler: alümina borosilikat, seramik nanoelyaflar, çöz-pel elektrospinleme, nanoteknoloji.

To My Exceptional Family

ACKNOWLEDGEMENTS

I would like to express my sincere gratitude to Prof. Dr. Güngör Gündüz for accepting me as my supervisor and for giving me such opportunities to fulfill this research. Additionally, I would like to thank my co-supervisor Prof. Dr. Uner Çolak for helping me on many occasions.

I would like to acknowledge Bora Maviş for his ideas and benefit to push this study further.

I would also like to thank Cengiz Tan and Nedret Özkar for their helps in characterization studies, Çiğdem Platsu for her help supplying the chemicals and equipment and the technicians of the machine shop for their helps.

I acknowledge with thanks the support of TÜBİTAK (The Science and Technical Research Council of Turkey)-MAG (Engineering Research Group).

I would like to give my most special thanks to my family, for being patient and understanding throughout my education period and for supporting me in whatever decision I've made.

Last but not least, I would like to thank all of my friends for all their emotional support and motivation during this extremely difficult accomplishment.

TABLE OF CONTENTS

PLAGIARISM.. iii

ABSTRACT iv

ÖZ.. iv

DEDICATION viii

ACKNOWLEDGEMENTS ix

TABLE OF CONTENTS x

LIST OF TABLES xiii

LIST OF FIGURES xiv

NOMENCLATURE xvii

CHAPTER

1. INTRODUCTION...1

2. LITERATURE SURVEY 4

2.1 Electrospinning 4

2.1.1 Fundamental Principles...4

2.1.2 Electrospinning Process..7

2.1.2.1 Schematic Setup of Electrospinning Electrospinning ……………………………………………………………………..8

2.1.2.2 Electrospinning Stages…………………………………9

2.1.2.2.1 Jet Initiation…………………………………………9

2.1.2.2.2 Jet Thinning……………………………………..11

2.1.2.2.3 Solidification of the jet…………………………13

2.1.3 Nanofiber Materials .. ……………………………………13

2.2 The Sol-Gel Chemistry 18

2.2.1 Catalyst Effect 21

2.2.2 Reactivity of various metal alkoxides 21

2.2.3 Influence of water 22

2.2.4 Influence of solvent... 22

2.2.5 Advantages of Sol-Gel Processing.......................... 23

2.2.6 Limitations of Sol-Gel Processing............................ 24

2.3 Formation Of Multicomponent Oxides............................... 25

2.4 Alumina Borosilicate Ceramic Systems............................. 26

3. EXPERIMENTAL 28

3.1 Introduction.. 28

3.2 Raw Materials... 28

3.3 Sol Preparation... 29

3.4 Electrospinning... 34

3.5 Heat Treatment... 35

3.6 Parameter Examined 35

3.7 Chemical Characterization... 35

3.7.1 Fourier Transform Infrared (FTIR) Spectroscopy......... 35

3.7.2 Scanning Electron Microscopy (SEM).......................... 35

3.7.3 X-Ray Diffraction (XRD) 36

3.7.4 Differential Thermal/Thermogravimetric Analysis (DTA/TG 36

4. RESULTS AND DISCUSSION.. 37

4.1 Preliminary Experimental Results...................................... 37

4.2 Parametric Studies 43

4.2.1 Effects of Viscosity and Solvent 43

4.2.2 Effect of Applied Electric Voltage 46

4.2.3 Effect of Tip-to-Collector Distance................................ 47

4.3 Sintering Effects.. 49

4.4 Fourier Transform Infrared (FT-IR) 55

4.5 X-Ray Diffraction (XRD).. 57

4.6 Differential Thermal and Thermogravimetric Analysis (DTA/TG) 59

5. CONCLUSIONS... 61

RECOMMENDATIONS 63

REFERENCES 64

LIST OF TABLES

Table

2.1 Examples of electrospun polymers 13

2.2 Ceramics that have been electrospun 17

3.1 Properties of the raw materials 29

3.2 Compositions of electrospinning solution #1 32

3.3 Compositions of electrospinning solution #2 32

3.4 Compositions of electrospinning solution #3 32

4.1 Viscosities of three different electrospinning solutions 43

4.2 Fibers diameters of various samples electrospun at 8, 10, 12 and 15 kV applied electric voltage 47

4.3 Fibers diameters of various samples electrospun at 7, 10, and 15 cm tip-to-collector distance 47

LIST OF FIGURES

Figure

2.1 The mechanism of the droplet explosion 7

2.2 A typical experimental setup of the electrospinning process 9

2.3 Schematic of the forces on a droplet at the tip of the pipette 11

2. 4 Sol-Gel Process 20

3.1 Flow chart of the synthesis of the Alumina borosilicate ceramic nanofibers.. 31

3.2 Electrospinning System 34

4.1 SEM micrographs of aluminum borosilicate/PVA electrospun fibers prepared by using aluminum ethoxide and toluene... 38

4.1 (contd') SEM micrographs of aluminum borosilicate/PVA electrospun fibers prepared by using aluminum ethoxide and toluene 39

4.2 SEM micrographs of aluminum borosilicate/PVA fibers prepared by using aluminum isopropoxide and isopropyl alcohol.. 41

4.2 (contd') SEM micrographs of aluminum borosilicate/PVA fibers prepared by using aluminum isopropoxide and isopropyl alcohol.................................... 42

4.3 SEM micrographs of PVA/alumina borosilicate fibers electrospun from solution with viscosity of 2.42 poise (Electrospinning solution #1)... 44

4.4 SEM micrographs of PVA/alumina borosilicate fibers electrospun from solution with viscosity of 6.5 poise (Electrospinning solution #2)... 45

4.5 SEM micrographs of PVA/alumina borosilicate fibers electrospun from solution with viscosity of 4.6 poise (Electrospinning solution #3)... 45

4.6 SEM micrographs of PVA/alumina borosilicate fibers electrospun at 15cm tip-to-collector distance and various electric voltages: (a) 8 kV; (b) 10 kV; (c) 12 kV; (d) 15 kV. 46

4.7 SEM micrographs of PVA/alumina borosilicate fibers electrospun at 10kV electric voltage and various tip-to-collector distances: (a) 7cm; (b) 10 cm; (c) 15cm. 48

4.8 SEM micrographs of alumina borosilicate/PVA composite fibers 50

4.9 Frequency distribution for fibers: (a) dried at 70°C (b) sintered at 800°C. 51

4.10 SEM micrographs of alumina borosilicate fibers sintered at 800°C 52

4.11 SEM micrographs of alumina borosilicate fibers sintered at 1000°C 53

4.12 SEM micrographs of alumina borosilicate fibers sintered at 1200°C 54

4.13 FT-IR spectra of various fiber samples: (a) As-dried at 70°C alumina-borosilicate/PVA composite fibers; (b) sintered at 800°C; (c) sintered at 1000°C. 56

4.14 XRD results of various fiber samples: (a) As-dried at 70°C alumina-borosilicate/PVA composite fibers; (b) sintered at 800°C; (c) sintered at 1000°C........................... 58

4.15 TG-DTA curves of precusor fibers of alumina borosilicate/PVA fibers.. 60

NOMENCLATURE

A^o	Amstrong
cm	Centimeter
C	Celcius
gr	Gram
k	Kilo
μ	Micron
mm	Millimeter
nm	Nanometer
V	volt

δ	Partial Charge
ε_o	Dielectric Permeability Of Free Space
F_e	Coulombic Repulsion Force
γ	Surface Tension
H	Tip-to-Collector Distance
L	Length of the Capillary
n	Coordination Number
Q	Droplet Charge
λ	Wavelength
R	Radius
θ	Theta
Vc	Critical Voltage
X	Fissility
z	Oxidation State

EtOH	Ethanol
FT-IR	Fourier Transform-Infrared Spectroscopy
i-PrOH	Isopropyl Alcohol
M	Metal
PVA	Poly Vinyl Alcohol
PVAc	Poly Vinyl Acetate
SEM	Scanning Electron Microscope
TEOS	Tetra Ethoxy Orthosilicate
TG-DTA	Thermogravimetric/Differential Thermal Analysis
XRD	X-Ray Diffractometry

CHAPTER 1

INTRODUCTION

Nanotechnology is nowadays a popular interdisciplinary field including many areas such as mechanics, electronics, optics, biology, medicine, and material science. “Nanotechnology” is the application of science to build the new materials or devices by manipulating and working with atoms and molecules down on the scale. The “nano” in nanotechnology means one billionth that is about 10,000 times smaller than the diameter of a human hair.

American physicist and Nobel Prize winner, Richard Feynman is accounted as the inspirational father of nanotechnology for introducing the idea of molecular manufacturing, in a lecture, “There is Plenty of Room at the Bottom” [1] in 1959. However, the origins of nanotechnology did not occur until then. He attracted his audience’s attention suggesting that what if one could build materials and devices with manipulating and controlling them at the molecular level.

In 1974, Norio Taniguchi introduced the term “nanotechnology” to represent extra-high precision and ultra-fine dimensions, and also predicted improvements in integrated circuits, optoelectronic devices, mechanical devices, and computer memory devices. This is the so-called ‘top-down approach’ of carving small things from large structures. In 1986, K. Eric Drexler in his book “Engines of Creation” discussed the future of nanotechnology, particularly the creation of larger objects from their atomic and molecular components, the so-called “bottom-up approach”. He proposed ideas for “molecular nanotechnology”, which is to produce any kind of object from elemental particles. [2]

Today, ceramic, polymer, and composite nanofibers and nanotubes are the most charming materials for nanotechnology. Because of their small characteristic dimension, high surface area, and microstructural features, they provide unique mechanical, optical, electronic, magnetic, and chemical properties for a wide variety of materials and applications. They are mostly produced by synthetic bottom-up methods resulting as discontinuous fibers. However, this method leads to difficulties with their alignment, assembly, and processing into applications. It is seen that continuous fibers provide easy alignment, assembly and processing because of superior mechanical properties (e.g., strength, stiffness etc.) and continuity of fibers. That’s why; there is a considerable interest in producing continuous fibers at nanoscale. “Electrospinning” as a top-down method makes possible the production of continuous and very narrow diameter range (10-1000nm) fibers efficiently. In the electrospinning process, there are two major components: a high voltage DC power supplier, a capillary tube with a small diameter, and a metal collection system. High voltage power supplier produces a high voltage electric field between an oppositely charged solution contained in a pipette and metallic collection screen. When the voltage attains a critical value, the suspended solution with hemi-spherical surface formed on the tip of the pipette ejects a charged jet. As the charged jets are spun, the fibers are collected as a randomly oriented, nonwoven mat on the surface of the metal collector.

A number of polymer nanofibers have been electrospun directly from polymer solutions or melt [3-10]. Recent studies demonstrate that ceramic and ceramic/ polymer composite nanofibers are also prepared with electrospinning using conventional sol-gel method, followed by a high-temperature pyrolysis [11-32]. The outcome of ceramic nanofiber studies will be utilized in many areas in the future, for example, nanostructured membranes for filtration and separation, reinforcement materials for nanocomposites, supports for nanostructured catalysts, and electrode materials for energy conversion or storage.

In this study alumina borosilicate/PVA composite nanofibers in composition of 0.8 SiO_2. 0.1 Al_2O_3 .0.1B_2O_3 were prepared using sol-gel method and electrospinning technique and characterized using SEM, XRD, FT-IR and DTA/TG techniques.

CHAPTER 2

LITERATURE SURVEY

In this part, the principles of electrospinning are presented with reviews of some polymeric and ceramic nanofiber materials published in literature. Also, conventional sol-gel method, which is used for the preparation of ceramic nanofibers via electrospinning, is explained.

2.1 Electrospinning

2.1.1 Fundamental Principles

English physicist Lord Rayleigh introduced the foundations of electrospinning, at the end of the 19th century. He studied theoretical behavior of isolated charged water droplets in thunderstorm cloud. There are two forces that influence a droplet: the Coulombic repulsion force (F_e) and the surface tension (γ) that give the droplet a spherical shape. Lord Rayleigh suggested that, at “Rayleigh limit” [33] these forces are equal and the system is stable.

Rayleigh Limit:

$$\mathrm{X} = \frac{\mathrm{Q}}{8\pi\sqrt{\varepsilon_o \gamma R^3}} = 1 \tag{1}$$

Where Q is the droplet charge, R is the droplet radius, γ is bulk liquid surface tension, ε_0 is the dielectric permeability of free space, and X is "fissility". As shown in Figure 2.1, when the solvent evaporates, the net charge density on the surface will increase and finally the electrostatic Coulomb repulsion forces become sufficient to overcome the stabilizing effect of the surface tension that holds the droplet together, the droplet becomes unstable and explodes into smaller droplets of equal charge. In other words when X>>1, an instability occurs and "the liquid is thrown out in fine jets, whose fineness, however, has a limit" [33]. Rayleigh's explosion study illuminated evolution of "electrospraying phenomenon (or electrostatic atomization)" which is the origin of fundamental principle of "electrospinning phenomenon".

Zeleny [34] studied the surface behavior of a charged droplet and demonstrated the effect of strong electrical potential applied to a small capillary tube, which induces the eventual break-up of jet from the droplet. Vonnegut and Neubauer [35] proved that it was possible to produce monodisperse particles below 1 micrometer from a pending droplet by the electrospraying technique. In the 1960s, Sir Geoffrey Taylor [36] obtained the critical electrical potential needed for the formation of a jet transformed from the droplet at the tip of a capillary tube and for the first time, he explained the cone shape of the pendant droplet which is attached to the capillary. He determined the cone angle, as 49.3° when the critical electrical potential was acquired and a jet of liquid was ejected from the tip. He derived an expression for the critical electrical potential needed to transform the droplet into the cone as:

$$V_c^2 = 4\frac{H^2}{L^2}\left(\ln\frac{2L}{R} - \frac{3}{2}\right)(0.117\,\pi\gamma R)$$

where *Vc* is the critical voltage, *H* is distance between the capillary exit and the ground, L is length of the capillary with radius *R*, and *γ* is the surface tension of the liquid. This cone is commonly known as “Taylor cone” and has an important role to the jet formation in both fiber and droplet formation processes. Hendricks et al. [37] found a similar relation for the electrospraying as:

$$V = 300 \sqrt{20 \pi \gamma r} \tag{3}$$

where *r* is the radius of pendant droplet. Even though they aren’t demonstrated in these two equations, both conductivity and viscosity have an important role in this process [38]. In 1986, Hayati et al. [39] made studies about mechanism of the stable jet formation. They concluded that conductive liquids, such as water caused to produce unstable jets moving to different direction, with further increase of the voltage. Semi-conducting and insulating liquids such as paraffinic oil produced the desired stable jet from a conical base. Since they cannot hold the surface charges, electrostatic forces cannot build up. Therefore, when the voltage is increased, the electrical potential difference between the cone base and its apex increases. In conclusion a tangential electric field is presented on the cone surface in the direction of the flow and the jet formed comes apart from the pendant droplet.

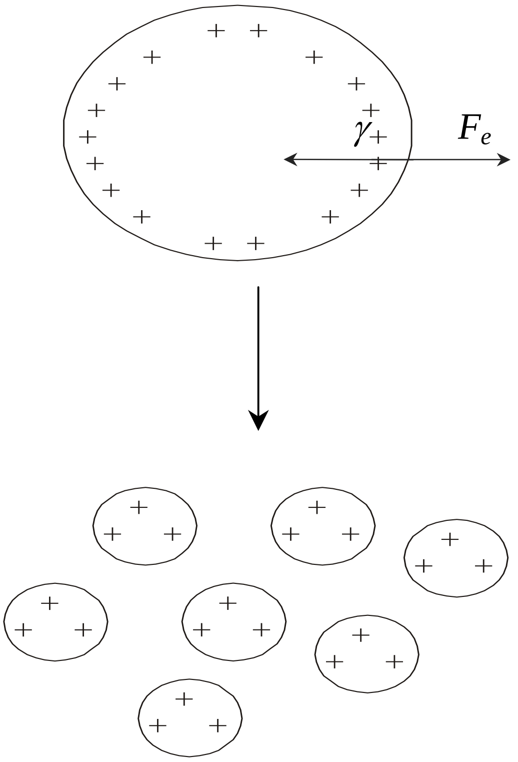

Figure 2.1 The mechanism of the droplet explosion

In electrospraying studies, many parameters like applied potential, capillary diameter; liquid properties like surface tension, conductivity, and viscosity have been investigated until now and they have facilitated in understanding the principles of the electrospinning process.

2.1.2 Electrospinning Process

Electrospinning is a novel approach for fiber production by employing electrostatic forces to drive the fiber formation process. Although electrospinning was developed in 1934 by Anton Formhals [40] who received the patent of the process, up to 1990s there had not been many publications. In 1971, Baumgarten [41] accomplished electrospinning of acrylic fibers ranging from diameters of 0.05 microns to 1.1 microns. Larrondo and Manley [42-44] studied the electrospinning of polyethylene and polypropylene fibers from polymer melts. They determined that the fiber diameter decreased with increasing the temperature of melt and electrical voltage applied. In 1995, Reneker et al [45-46] investigated electrospinning process parameters in detail for production of polyethylene oxide (PEO) solution fibers with diameters ranging form 0.05 microns to 5 microns and observed that stable fibers were obtained at high viscosity of solutions. And then, this technique became fetching due to the likely application areas including nanocomposites, optics, electronics, tissue engineering, medical, and other industrial and functional products.

2.1.2.1 Schematic Setup of Electrospinning

A typical experimental setup of the electrospinning process is shown in Figure 2.2. A capillary pipette contains a solution, which is connected to a high voltage power source through a copper wire serving as a positive electrode. A metal collector serving as a counter electrode is placed against the pipette. When a high voltage applied between the capillary and the collector reaches a critical value, an electrically charged jet of solution pulled out of the tip of the pipette and fibers are collected on the metal collector [45]. Just before the critical value, the electrical force almost overcomes the surface tension of liquid, the surface of the drop suspended at the tip of pipette forms a Taylor cone [36], as cited previously. The jet emerges from the tip of this cone and then is elongated into thin filaments with splaying [45] or bending [47] process. Finally, at the distance between the tip and the collector, the solvent evaporates and the solidified fibers' diameters are extremely reduced.

Many parameters including solution characteristics (e.g., viscosity, elasticity, concentration, surface tension, net charge density, solvent, molecular weight) and process variables (e.g., electrical potential, distance between capillary tip and collector, diameter of the capillary tip, temperature, humidity, air flow in the electrospinning chamber) affect fiber size and morphology.

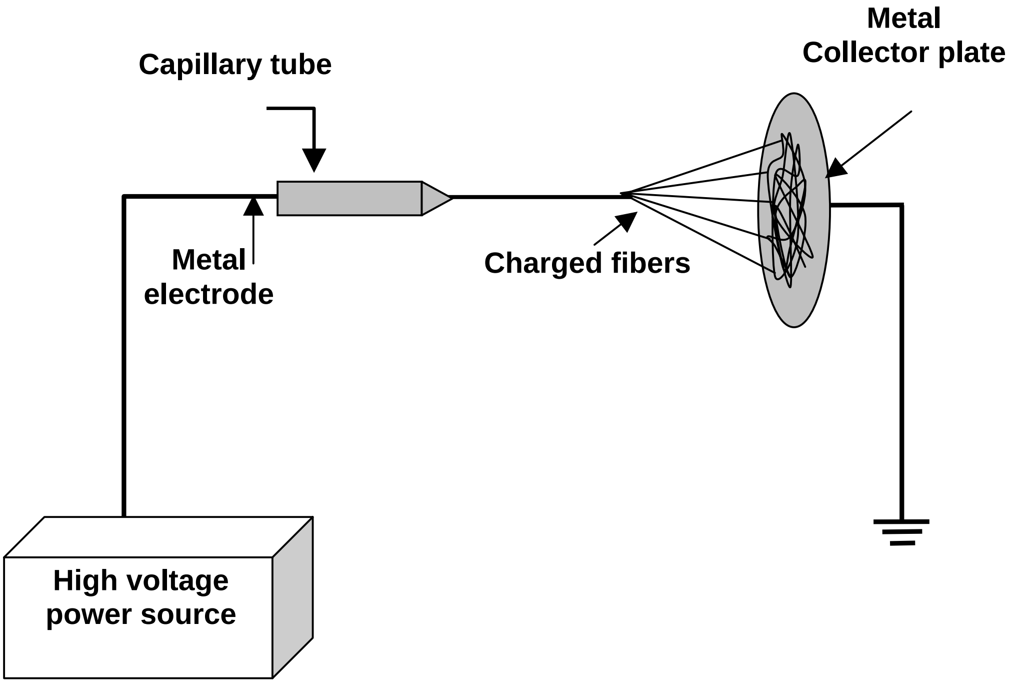

Figure 2.2 A typical experimental setup of the electrospinning process

2.1.2.2 Electrospinning Stages

The electrospinning process consists of three stages [48]:

1) Jet initiation/the cone formation
2) Jet thinning
3) Solidification of the jet following nanofiber formation.

2.1.2.2.1 Jet Initiation

Jet initiation from the droplet is the first stage of the electrospinning process. One of the electrodes is placed into the solution and the other is attached to the metal collector. When the high voltage is subjected to the solution, charges are induced on the surface of the droplet and they create radial electrical forces directly opposite of the surface tension due to the mutual charge repulsion. Overall there is a force balance on the droplet where gravity and electric polarization stress tend to elongate the droplet with tangential electric stress, viscosity of the fluid try to resist the formation of the cone, the surface tension try to minimize the surface area pulling the droplet surface and oppositely, the normal electric stress try to maximize the surface area (Figure 2.3). When the electric field is large enough, these forces distort the shape of the drop into a conical configuration known as the Taylor cone [36]. Further increasing the electric field, at some critical value, surface tension can no longer endure the electrostatic repulsive forces and the charged thin jet of the fluid is ejected from the surface of the Taylor cone. This jet is observed in a stable region and the length of the region is increased with increasing viscosity [41]. Taylor [36] found that the jet is formed when the cone angle attains 49.3° as mentioned previously, but recently Yarin et al. [49] determined that the cone angle just before the jet ejection should be 33.5° and Fong and Reneker found the cone angle as 22.5°, not 49.3° [48]. Doshi and Reneker measured the jet diameter as a function of distance from the apex of the cone [48]. They electrospan 4 wt% of poly (ethylene oxide) (PEO) at 10kV and demonstrated that the jet diameter decreased as a factor of 5 at a distance of 1cm from the cone apex, with increasing distance between the capillary tip and the metal collector.

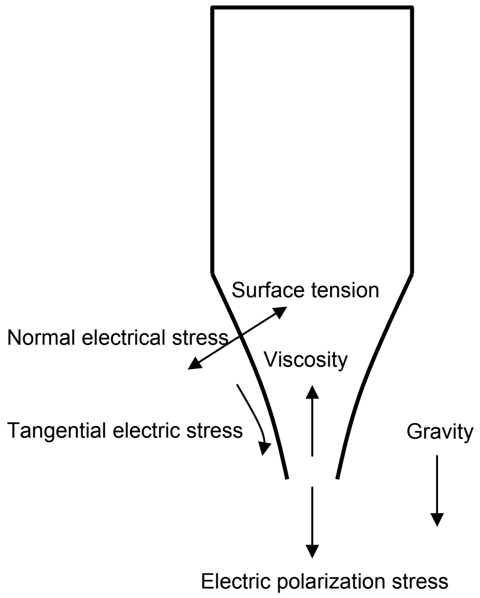

Figure 2.3 Schematic of the forces on a droplet at the tip of the pipette

2.1.2.2.2 Jet Thinning

Fluid instabilities occur in this stage. After some distance, the jet ejected from the tip of the cone continues rapidly towards the collector with some bending instability due to the repulsive electrostatic forces constituted by the charged ions in the jet [49]. It was believed that the stable jet splitting or “splaying” into multiple other jets due to the charge repulsion caused the bending instability [50]. They indicated that fiber diameters decreased due to the simultaneous stretching of the jet and the evaporation of the solvent resulting to the increase of the surface area, that is, the charge density. Similar to electrospraying process, the increase of the charge density split the jet into smaller jets then resulting in the formation of fibers with very smaller diameter [50]. Recent studies have suggested that the non-axisymmetric or whipping instability primarily causes the reduction of the jet diameter [6, 47, 51-

53]. Reneker et al. investigated the instability of electrospinning polyethylene oxide (of 6 wt%) and observed the path of the electrified jet [47]. After the jet traveled from a pendant droplet in a lateral position with bending, winding, and spiraling loops, these loops became longer and thinner due to the electrical forces. Shin et al. [51-53] also studied with PEO solution and confirmed that the jet observed to be splaying into multiple filaments is a single, rapidly whipping jet virtually. They, besides, identified the possibility for three different types of instabilities: (1) the classical Rayleigh mode instability which is axisymmetric (2) the axisymmetric conducting mode instability involves a purely electrical competition between free charge and the electric fields and (3) the nonaxisymmetric “whipping” mode instability. These instabilities vary depending on the fluid parameters and operating conditions.

When the electrical field is small, Rayleigh instability occurs. At further fields, the electrical instabilities are enhanced depending on the increase of the surface charge density and the decrease of the radius of the jet. First, the Rayleigh instability is suppressed and axisymmetric conducting mode occurs, then at high electrical fields the whipping instability dominates. The whipping instability accounts for the small diameters of fibers which can be produced via electrospinning. Both research groups (Shin et. al and Reneker et al.) observed the whipping or bending motion of electrospinning PEO jet without the splitting. However, some research groups observed the splaying or splitting phenomenon using more advanced experimental set-up. Deitzel et al. [54] observed a splaying event during the electrospinning of 10 wt% PEO solution. Also, some polymer solutions such as 16 wt% HEMA [poly(2-hydroxethyl methacrylate)], 30 wt% polystyrene, and 20 wt% poly(vinylidene fluoride) were electrospun into nanofibers and during the spinning process, the splitting phenomenon occurred. [55]

2.1.2.2.3 Solidification of the jet following nanofiber formation

The final stage is the solidification of the jet into nanofibers. The jet continues to expand the rapid bending and/or splaying forming thinner jets and finally arrives to the metal collector. Many parameters such as tip-to-collector distance, the collector, applied field, concentration etc. influence the fiber diameter, distribution, and morphology but in solidification process the effects of these have not been understandably investigated.

2.1.3 Nanofiber Materials

Throughout history, in the mid 1990's, many functional polymers have been electrospun into nanofibers. Table 2.1 shows some of the examples of the polymers, which have been successfully spun into nanofibers.

Table 2.1 Examples of electrospun polymers.

Polymer	**Solvent**	**Reference**
Polyvinyl alcohol	Distilled water	[3]
Polystyrene	Tetrahydrofuran	[4]
Cellulose Acetate	Acetone, Acetic acid, Dimethylacetamide	[5]
Polyethylene oxide	Water	[6]
Polyurethane	Dimethyl formamide	[7]
DNA	Water, ethanol	[8]
Collagen	Hezafluoro-2-propanol	[9]
Polyethylene terephthalate	Melted at 270 ^{o}C	[10]

Despite electrospinning has been applied to many organic polymers due to their favorable viscoelastic behavior, recent studies have demonstrated that continuous ceramic and composites materials can also be fabricated by electrospinning. Continuous ceramic fibers demonstrate appealing properties such as high strength, elastic modulus with high-temperature capability and a general freedom from environmental attack. Ceramic nanofibers can be produced by various techniques including chemical vapor deposition, polymer pyrolysis, co-precipitation (PPT), sol-gel etc. But among these techniques, PPT and sol-gel routes, which also described as wet-chemical synthesis techniques, are preferred for electrospinning applications, because of their several advantages such as control of crystallinity, grain/crystal size, shape, morphology, and stoichiometry. Both techniques use metal-organic precursors, but there are distinct difference between these two techniques in the type of precursors and the reaction mechanism. PPT utilizes salts of nitrates, carbonates, halogens, or oxalates, and sol-gel utilizes metal alkoxides. Basically, precursors are mixed with a solvent and polymer and are then electrospun into fibers. After electrospinning, nanofibers are introduced into a high temperature heat treatment process to remove the organic phase and finally to obtain pure ceramic nanofibers. The function of the polymer is to increase the viscosity, thus to affect electrospinnability of the solution.

Shao and his coworkers first prepared silica nanofibers by sol-gel processing and electrospinning technique using TEOS and PVA [11]. After calcination of thin fibers, organic phase were removed and amorphous silica nanofibers with diameters of 200-300 nm were obtained. These fibers were characterized by the (SEM), (FT-IR), and (XRD). The results showed that silica nanofibers in the amorphous state formed at 550°C. Dai et al. prepared alumina-borate nanofibers using aluminum stabilized with boric acid and PVA solution. After calcination, alumina-borate oxide ultra-fine fibers were obtained [12]. The characteristic results demonstrated that at 1000-1200°C, $Al_4B_2O_9$ and $Al_{18}B_4O_{33}$ formed and decomposed above 1400°C because of the instability of alumina-borate. At 1400°C the stable crystalline phase of α-Al_2O_3 were seen. The SEM results showed that the grain size of the fibers were small at 1000°C and increased at 1200°C, due to the coalescence of the grains. The grains disappeared and the surface of the fibers at 1400°C became smoother due to the formation of a homogeneous α-Al_2O_3 crystalline phase. The characteristics of the microstructure suggested that liquid phase sintering occurred in the product because of the firing treatment.

Choi et. al. [13] prepared nanofibers of titania-doped silica fibers by electrospinning of tetraethyl orthosilicate/titanium(IV) isopropoxide sol without a gelling agent (or binder). After characterizing the nanofibers, the results indicated that titania-doped silica fibers did not have crystalline structure even after the temperature of 1000°C.

Viswanatheemuntie et. al. [14] prepared niobium oxide fibers using niobium ethoxide and poly vinyl acetate (PVAc); germanium oxide nanofibers [15] using germanium isopropoxide PVAc; and, vanadium oxide nanofibers [16] using vanadium oxide isopropoxide and again PVAc followed by thermal treatments. It was observed that both the morphologies and the crystallinities of the fibers depended on the calcination temperature.

Yang et. al. [17] electrospan thin PVA/cerium nitrate composite fibers using the solutions of cerium nitrate and PVA, for the first time. After calcination CeO_2 nanofibers with a diameter of 50-150 nm were successfully obtained.

Yu et. al. [18] prepared extra thin fibers of PVA/lithium chloride/manganese acetate composite fibers through sol-gel and electrospinning. After calcination of the precursor at 600°C, the spinel lithium manganese oxide ($LiMn_2O_4$) nanofibers, with a diameter of 100-200 nm, were successfully obtained.

Wang et. al. [19] synthesized micro/nanoscopic $Pb(Zr_{0.52}Ti_{0.48})O_3$ fibers from zirconium propoxide, titanium isopropoxide, and lead (II) ethylhexaonate. After sintering of electrospun fibers, the fibers diameter was observed varying from several hundreds of nanometers to about 10 μm.

Park [20] fabricated lanthanum copper oxide nanofibers for using in toxic gas sensor applications. It was seen that the sensitivity and the response time of lanthanum copper oxide electrospun sensors was appreciably good compared to the same sensors produced with different process.

Recently, the first electrospun biomaterial ceramic fibers were produced. Wu et. al. have electrospun hydroxyapatite $Ca_{10}(PO_4)_6(OH)_2$ using a precursors of $Ca(NO_3)_2.4H_2O$ and $(C_2H_5O)_3PO$. After calcination at 600°C pure hydroxyapatite fibers with a diameter of 25μm were obtained. However, further investigation needs to be done to reduce the diameter [21]. In Table 2.1, some of the other ceramic fiber systems produced by electrospinning are presented.

Table 2.2: Ceramics that have been electrospun.

Ceramic	***Precursor electrospun fibers***	***Comments***	***Reference***
TiO_2	1. Titanium butoxide 2. P-123 (EO20-PO70-EO20) 3. HCl	Sol-gel	[22]
$MgTiO_3$	1. Magnesium ethoxide 2. Titanium isopropoxide 3. 2-Methoxyethanol in N_2 4. Polyvinylacetate in DMF	Sol-gel	[23]
$NiTiO_3$	1. Nickel acetate 2. Ethanol 3. HNO_3	Sol-gel	[24]
SnO_2	1. $C_{22}H_{44}O_4Sn$ 2. PEO 3. $CHCl_3$	Sol-gel	[25]
$BaTiO_3$	1. Barium acetate 2. Titanium isopropoxide 3. PVP 4. Ethanol 5. Acetic acid	Sol-gel	[26]
Co_3O_4	1. Cobalt acetate 2. PVA	Sol-gel	[27]
NiO/ZnO	1. Nickel acetate 2. Zinc acetate 3. PVA	Sol-gel	[28]
ZrO_2	1. Zirconium oxychloride 2. PVA	Sol-gel	[29]
$NiFe_2O_{4\_}$	1. Iron (II) ethylhexano isopropoxide 2. Nickel ethylhexano isopropoxide 3. Acetic acid 4. PVP	Sol-gel	[30]
Fe_3O_4	1. Iron (II) chloride + iron (III) chloride + graft copolymer 2. PEO or PVA	Co-precipitation	[31]
Mn_2O_3-Mn_3O_4	6. Manganese acetate 7. PVA	Sol-gel	[32]

2.2 The Sol-Gel Chemistry

The sol-gel process involves the transition of a system from a liquid "sol" (mostly colloidal suspension) into a 3-dimensional solid network "gel" phase. By applying this process, ceramic or glass materials are fabricated in many forms such powders, coatings, thin films, fibers, membranes, or monoliths as presented in Figure 2.4 This process uses inorganic metal salts or organo-metallic precursors such as metal alkoxides. The most commonly preferred precursors are metal alkoxides (M(OR)n), where M is a metal, R is alkyl group such as methyl (CH_3), ethyl (C_2H_5), propyl (C_3H_7), or butyl (C_4H_9), and n = the valence of the metal atom. The transition from sol to gel requires two reaction steps: hydrolysis and condensation of metal alkoxides. Hydrolysis reaction occurs with addition of water into the alkoxide system using an acid or a base as a catalyst. During hydrolysis, the alkoxy ligands (OR) are replaced by hydroxyl ligands (OH) of the water as seen below:

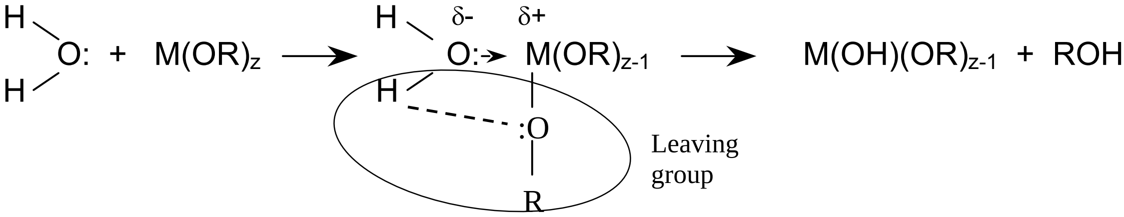

The whole process follows the mechanism of nucleophilic substitution in which a water molecule attacks the positively charged metal atom. Once partially or totally hydrolyzed, the metal hydroxides undergo a stepwise condensation with possible 3 competitive mechanism: alkoxolation, olation, and oxolation.

Alkoxolation with elimination of alcohol: MOH species coming from hydrolysis reacts with an alkoxide forming an oxo (-O-) bridge

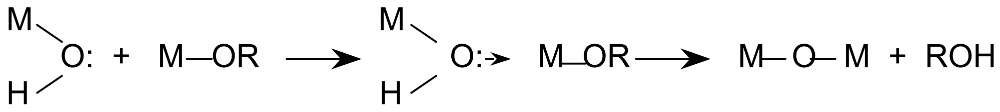

Oxolation with elimination of water: Two MOH species react to form an oxo bridge

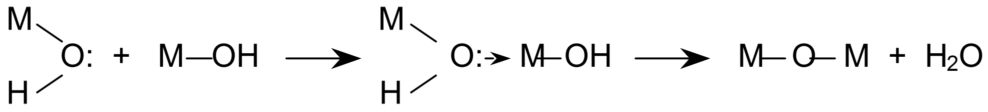

Olation with elimination of either alcohol or water: Either an alcohol molecule coming from a protonated alkoxy ligand or a water molecule coming from a protonated solvated alkoxide reacts with an MOH group resulting the formation of a hydroxo (-OH-) bridge.

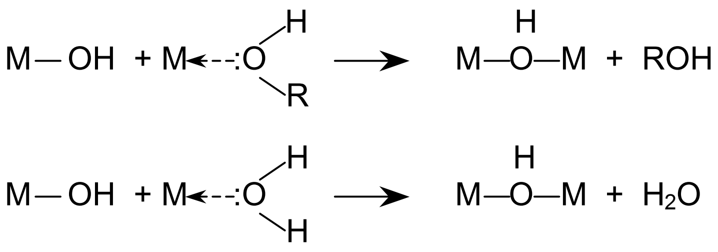

Hydrolysis and condensation reactions both gradually build up M-O-M linkages that, in turn, yield a viscoelastic, three-dimensional network (called gel) at the end [56]. It should be noted that, hydrolysis and condensation reactions occur concurrently, but one reaction can be favored over the other depending on the reaction conditions. That’s why a wide variety of reaction parameters are important in determining the physical properties and structures of these networks, e.g., catalyst, type of alkoxide, solvent, stoichiometry of water, stearic effects, and inductive effects [57].

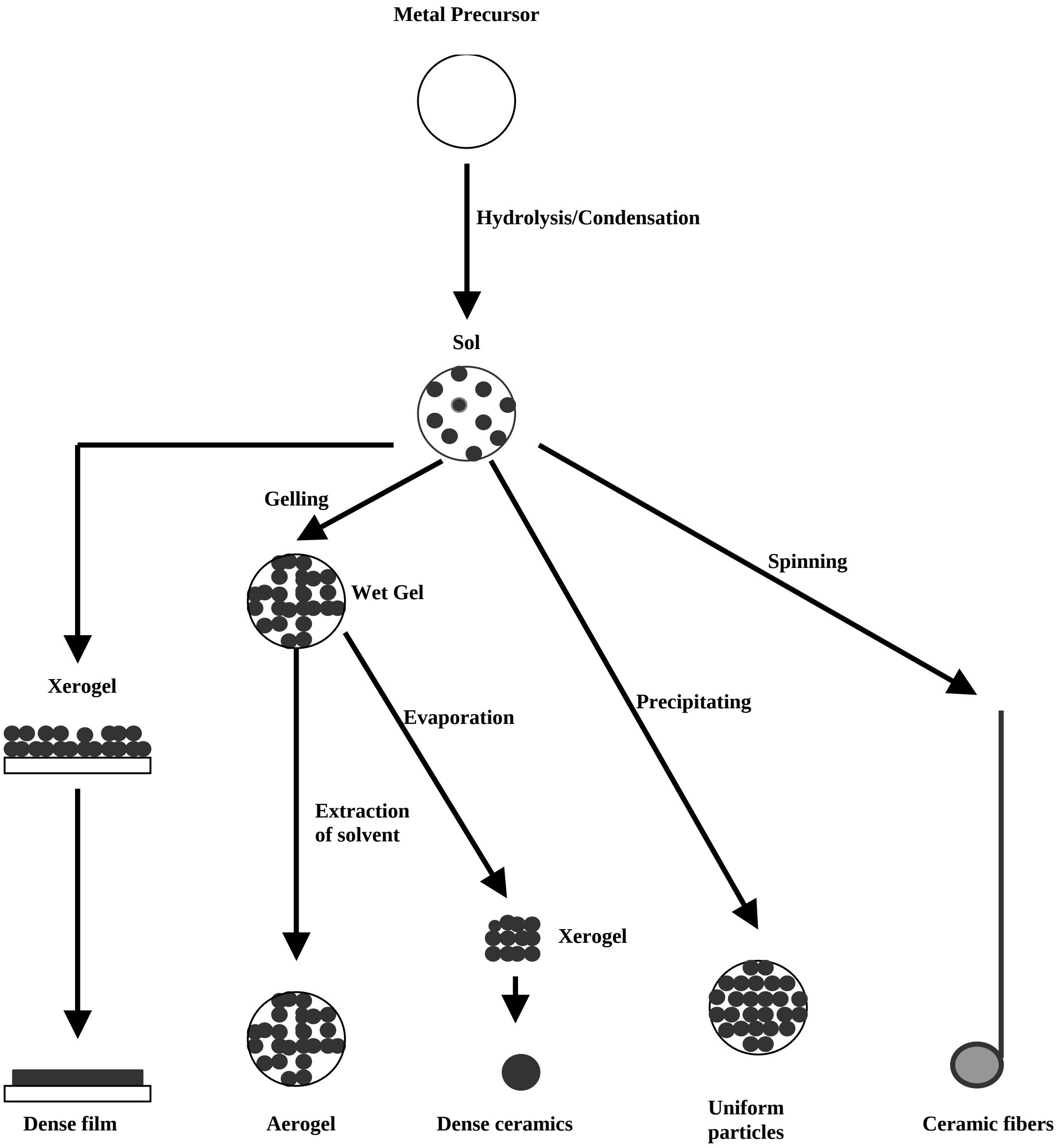

Figure 2.4 Sol-Gel Process

2.2.1 Catalyst Effects

In general, it has been shown that the catalyst provides control of the hydrolysis and condensation kinetics and therefore control of the gel morphology. In acid catalysis, hydrolysis rate is fasted up and condensation rate is considerably slowed down so, more linear-like chains with little branching are produced. In base catalyzed medium, both hydrolysis rate and condensation rate increase, therefore at early stages in the process where unhydrolysed alkyl groups are still present, branched chains or colloidal particle formation occurs [56].

2.2.2 Reactivity of various metal alkoxides

Except for $Si(OR)_4$, all alkoxides hydrolyse and condense extremely fast. This difference is explained by the nucleophilicity of the attacking group ($\delta(O)<<0$) and the electrophilicity of the metal atom ($\delta(M)>>0$). The partial charge of Si in $Si(OR)_4$ is smaller than that of the other metals in their corresponding alkoxides. It is consequently much harder to hydrolyse the silicon alkoxides compared to others [58]. Another well-accepted explanation for the reactivity of the tetravalent metal alkoxides $M(OR)_4$ is; if z is the oxidation state of the metal atom in the alkoxide, then one can define the degree of unsaturation of the metal atom as $n-z$, where n is the coordination number usually found in the oxide. Hence increasing the quantity $n-z$ denotes increasing the rate of hydrolysis reaction. For example, the tetra-coordinated alkoxide zirconium (IV) propoxide forms a network of ZrO_2 in which the zirconium is hepta-coordinated. This yields that n-z=3. Another tetra-coordinated alkoxide silicon (IV) propoxide also forms a network of SiO_2, in which the Si is tetra-coordinated. Thus, the degree of unsaturation n-z=0. Hence, hydrolysis reactivity for similar OR groups:

$Zr(OR)_4 >> Si(OR)_4$. Therefore, the hydrolysis rate of $Si(OR)_4$ must be catalyzed either by a strong electrophile such as H^+ or by a strong nucleophile such as OH^- [58].

2.2.3 Influence of water

Since water is a reactant in the sol-gel process, its presence plays an important role in the reaction kinetics and final morphology of the material. Actually, the main parameter that influences the hydrolysis reaction is the stoichiometric ratio of water per metal alkoxide ($[H_2O]:[M(OR)_z]$). Adding insufficient amounts of water for the reaction inclines to form a linear structure. Further increasing the amount of water leads the formation of more dense spherical particles [58].

2.2.4 Influence of solvent

The nature of the solvent used has a great influence on the overall reaction rate and the gel morphology. The solvents used in the sol-gel process may be categorized as polar-protic (i.e., methanol, water, and formamide), polar-aprotic (i.e., dimethylformamide, acetonitrile, and acetone) and non-polar-aprotic (i.e., dioxane, benzene, and hexane).

The aprotic solvents dissolve ionic compounds and they solvate cations very strongly but do not solvate anions to any appreciable extent so the left anions become highly reactive both as base and nucleophile. In addition, non-polarity does not tend to stabilize the reactants with respect to the activated complex. Therefore, non-polar-aprotic solvents enhance the condensation rate leading to the formation of large, dense spherical particles with long gelation time.

The polar aprotic solvents also do not hydrogen bond to the anions because of the aproticity, but the polarity stabilizes the anionic reactants with respect to the activated complex so the reaction rate is slowed down, gelation time decreased to some extent, and nominally condensed particles are formed.

The polar protic solvents decelerate the condensation rate. Protic solvents have hydroxyl groups and they dissolve ionic compounds because of electrostatic interactions between their partially negatively charged oxygens and cations, and between their partially positively charged hydrogen and anions. Hydrogen bonding to the anion of the reagent prevents an efficient condensation and as a result highly branched polymeric structure rather than dense particles are formed in a very short gelation time [57].

2.2.5 Advantages of Sol-Gel Processing

There are many significant advantages of the sol-gel processing:

1- This process occurs at low temperatures, frequently close to room temperature. Thus, thermal degradation of material is minimized, and high purity products are obtained.
2- By comparison with the classical high temperature synthesis of conventional ceramics, this low temperature process minimizes considerably the chemical interactions between the material and the container.
3- Very pure products are obtained by simply purifying the precursors such as metal alkoxides and mixed alkyl/alkoxides either by distillation, crystallisation, and electrolysis.
4- Highly porous materials and nanocrystalline materials can be prepared in this way.

5- Size, shape, and size distribution of colloidal particles can be easily controlled.
6- The low temperature of sol-gel is generally below the crystallization temperature for oxide materials, and this allows the production of unusual amorphous materials.
7- The optical quality of the materials is often good, leading to applications for optical components.
8- Since liquid precursors are used it is possible to cast ceramic materials in a range of complex shapes and to produce thin films or fibers as well as monoliths, without the need for machining or melting. [58]
9- Sol-gel processing offers the most outstanding advantages for mixed oxide systems in which the chemical homogeneity of the various elements can be controlled down to the atomic level. This is the case of the Lead Lanthanum Zirconium Titanates (PLZT) [59]. This condition is, however, virtually impossible to achieve when solid powders are mechanically mixed such as in the conventional processes; and hence the optical transparencies obtained are, in this case, not as high as those obtained by sol-gel processing [56].

2.2.6 Limitations Of Sol-Gel Processing

Despite all these advantages, there are some limitations of the sol-gel processing:

1- The precursors are often expensive and sensitive to moisture, limiting large scale productions plants
2- The process is time-consuming, particularly where careful ageing and drying are required.

3- The problems of dimensional change on densification, and of shrinkage and stress cracking on drying, although not insuperable, do require careful attention [56].

2.3 Formation Of Multicomponent Oxides

It is proposed that formation of soluble polymerazing species from alkoxides requires the presense of both “OR” and “OH” groups in the structure. On the other hand, the most of the alkoxides hydrolyze quite fast when contact with water by elimination of “OR” groups forming insoluble oxides and hydroxides which precipitate out of the solution. For example, aluminum alkoxides, $Al(OR)_3$, initially form the monohydroxide which tends to later convert to the trihydroxide [60].

$$Al(OR)_3 + 2H_2O \rightarrow AlO(OH) + 3R(OH) \qquad (4)$$

$$AlO(OH) + H_2O \rightarrow Al(OH)_3 \qquad (5)$$

Boron alkoxides react with water resulting the formation of boron oxide.

$$2B(OR)_3 + 3H_2O \rightarrow B_2O_3 + 6R(OH) \qquad (6)$$

These two types of hydrolysis reactions cannot make further condensation reactions due to the high hydrolysation rate of these alkoxides. Yoldas found that reactions 1, 2, and 3 can be manipulated by diluting the alkoxide and the water with alcohol before mixing; in this manner condensation reactions can occur [60]. Another type of hydrolysis reaction, exhibited by silicon alkoxides, forms neither oxide nor hydroxide upon completion, even in excess water. Unlike the other reactions, a soluble complex where “OH” or “OR” groups coexist in significant numbers is formed due to the slow hydrolysation of silicon alkoxides[60]. The partially hydrolysed complex is suitable for condensation reactions.

For formation of multicomponent oxide system, the preferred way is to start from an alkoxide, which hydrolyses and condensates slowly. After the slow hydrolyzing alkoxide is partially hydrolyzed, the faster hydrolyzing alkoxide is introduced to the solution by direct contact with partially hydrolyzed bonds of other alkoxides and finally homogeneous oxide system is attained, e.g.:

$$\equiv\text{Si-(OH)} + \text{(OR)-Al=} \rightarrow \equiv\text{Si-O-Al=} + \text{ROH} \quad (7)$$

2.4 Alumina Borosilicate Ceramic Systems

Alumina, silica and boron oxide based fiber systems have been studied by many authors [61-66] due to they represent a group of interesting properties which may be used in various applications including overheating protection, reinforcing medium for composite materials, and adsorbents in diesel engine filters. Alumina fibers, which have poor mechanical properties at high temperatures but have good durability and mechanical properties in oxidizing environments, have previously been successfully prepared using melt cooling, sol-gel [61,62]. Alumina borate fibers have attracted more attention due to their stability at high temperature. Readey [66] produced $Al_{18}B_4O_{33}$ whisker-like grains and found that aluminum borate phase was stable up to 1700°C. Dai et. al. [12] have electrospun alumina-borate oxide system into ultra-fine nanofibers which may have the potential for use as ceramic filters and ceramic-metal composite performs. Silica nanofiber, which have good unique properties and promise for applications such as mesoscopic research and optoelectronic devices can also be electrospun successfully [11]. So far, to our knowledge, there has been no study about alumina borosilicate ceramic fibers. In this work, alumina borosilicate ceramic nanofibers were prepared using both sol-gel and electrospinning techniques. Finally, heat treatment was applied on fibers to obtain pure, fine, dense alumina borosilicate ceramic fibers and characterization was carried out by SEM, XRD, FT-IR, and DTA-TG analyses.

CHAPTER 3

EXPERIMENTAL

3.1 Introduction

Aluminum borosilicate ceramic nanofibers with compositions of $0.8SiO_2.0.1Al_2O_3.0.1B_2O_3$ were prepared by using the sol-gel method and the electrospinning technique. The preparation procedure consists of three steps, sol preparation, electrospinning, and heat treatment.

3.2 Raw Materials

Raw materials used to prepare the electrospinning solution are; tetraethyl orthosilicate $Si(C_2H_5O)_4$ with a purity of greater than 98%, and triethyl borate $B(C_2H_5O)_3$ with a purity of greater than 99% from MERCK, aluminum isopropoxide $Al(C_3H_7O)_3$ with a purity of 97%, hydrochloric acid from Aldrich Chemical Co., and absolute ethanol with a purity of 99.5% from Gurup Deltalar as a solvent. Physical properties of these materials are listed in Table 3.1. Double distilled water was used for hydrolysis reaction.

Table 3.1 Properties of the raw materials.

	Formula	Molecular Weight	Density (g/ml)	Appearance
Tetraethyl orthosilicate	$Si(C_2H_5O)_4$	208.33	0.94	Liquid
Aluminum isopropoxide	$Al(C_3H_7O)_3$	204.25	–	Powder
Triethyl borate	$B(C_2H_5O)_3$	145.99	0.858	Liquid
Hydrocloric acid	HCl	36.46	1.2	Liquid
Absolute Ethanol	C_2H_5OH	46.07	0.798	Liquid
Isopropyl alcohol	C_3H_7OH	60.09	1.78	Liquid

3.3 Sol Preparation

In this study, Alumina borosilicate/PVA composite solution was prepared by using sol-gel method.

In the first stage of this study, aluminum ethoxide as aluminum source and toluene as solvent were used. However, aluminum ethoxide is a fast precipitating material and toluene is a non-polar and aprotic solvent hence, fast gelation prevented to occur the electrospinning process to slow down the reaction kinetics and to prevent fast gelation, aluminum isopropoxide precursor, which has larger alkoxy groups, was used instead of aluminum ethoxide and isopropyl alcohol (i-PrOH), which is polar and protic solvent was used instead of toluene.

Briefly, aqueous PVA solution was prepared by dissolving PVA powder in distilled water and heating at 80°C by stirring for 1 h, then cooling to room temperature and stirring for 24 h. TEOS was partially hydrolyzed before the addition of aluminum isopropoxide and triethyl borate. In this partial reaction, TEOS was mixed in absolute ethanol in a beaker. Then, HCl/H_2O solution was dropped slowly to the TEOS/ethanol solution under vigorous stirring (Solution A). TEOS and water are immiscible at all proportions. This is done because EtOH makes TEOS and water miscible and thus facilitates hydrolysis, which takes place as follows,

$$Si(OC_2H_5)_4 + H_2O \rightarrow HO\text{-}Si(OC_2H_5)_3 + C_2H_5\text{-}OH$$

Ethanol is the byproduct of this reaction and partially hydrolyzed silanol complexes are obtained. After one hour, the solutions including triethyl borate and aluminum isopropoxide were prepared. For the preparation of aluminum isopropoxide solution, first PVA is placed into a beaker, and then some amount of HCl was added into the polymeric solution. Finally, aluminum isopropoxide was added into the solution with its parent alcohol (isopropyl alcohol) and it was mixed until the transparent solution (Solution B) formed. The triethyl borate solution (Solution C) was prepared in the same manner: PVA was placed in a baker, and then some amount of HCl was added into the PVA solution. Finally boron ethoxide was added into the solution with its parent alcohol (ethanol), and was mixed until the transparent solution formed. These three solutions were stirred all together and the final mixture was electrospun into nanofiber. In Figure 3.1, the entire experimental procedure from preparing the electrospinning solution to obtaining ceramic nanofibers is summarized.

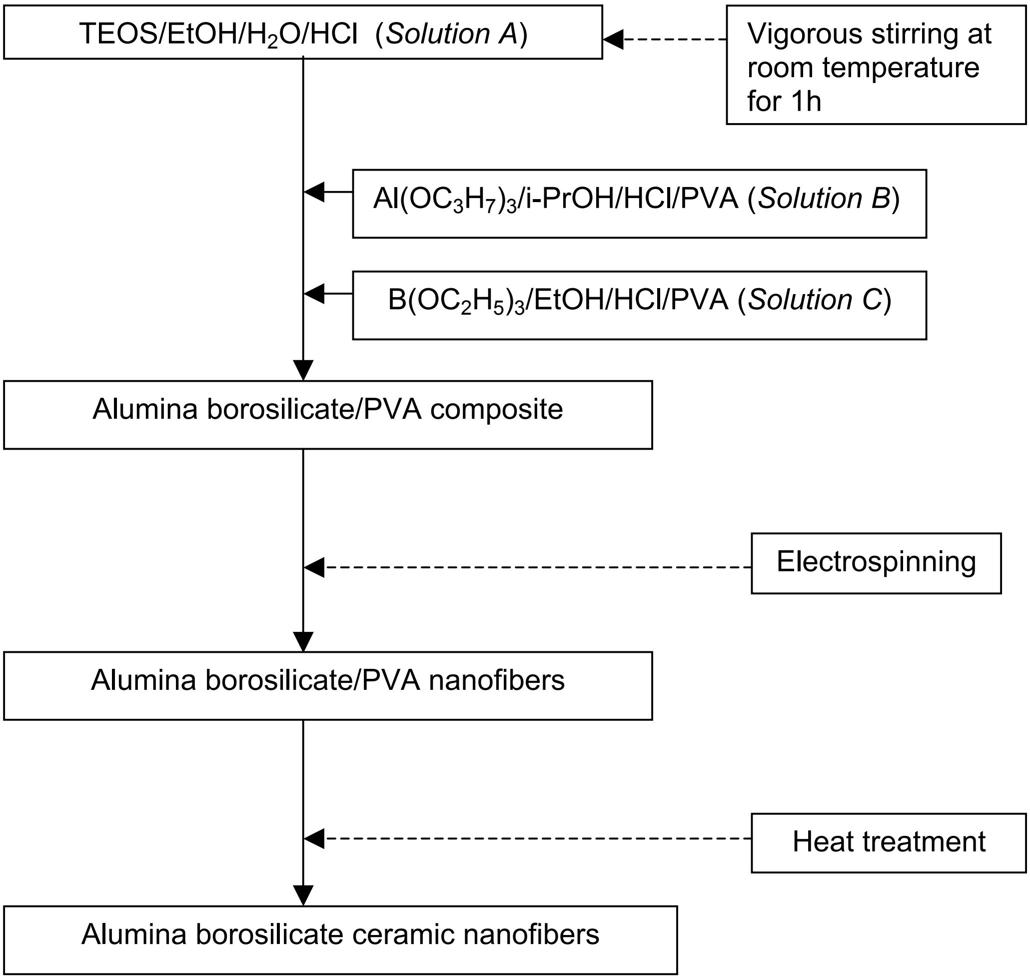

Figure 3.1 Flow chart of the synthesis of the Alumina borosilicate ceramic nanofibers

Alumina borosilicate fibers were prepared from tetraethyl orthosilicate (TEOS), aluminum isopropoxide ($Al(OC_3H_7)_3$), and triethyl borate ($B(OC_2H_5)_3$). They were mixed at the appropriate molar ratios to obtain a final compound of $0.8SiO_2.0.1Al_2O_3.0.1B_2O_3$. Table 3.2 to 3.4 gives the recipe of three solutions for electrospinning. All these solutions yield the same final product, i.e. '$0.8SiO_2.0.1Al_2O_3.0.1B_2O_3$', but, they have different viscosities.

Table 3.2 Compositions of electrospinning solution #1

Solution A	TEOS:EtOH:H_2O:HCl	1:10:2:0.01 (molar ratio)
Solution B	$B(C_2H_5O)_3$:EtOH:HCl	1:10:8 (molar ratio)
	($B(C_2H_5O)_3$:EtOH:HCl): PVA	1:1 (weight ratio)
Solution C	$Al(C_3H_7O)_3$:i-PrOH:HCl	1:20:8 (molar ratio)
	($Al(C_3H_7O)_3$:i-PrOH:HCl):PVA	1:1 (weight ratio)

Table 3.3 Compositions of electrospinning solution #2

Solution A	TEOS:EtOH:H_2O:HCl	1:10:2:0.01 (molar ratio)
Solution B	$B(C_2H_5O)_3$:EtOH:HCl	1:10:8 (molar ratio)
	($B(C_2H_5O)_3$:EtOH:HCl): PVA	1:3 (weight ratio)
Solution C	$Al(C_3H_7O)_3$:i-PrOH:HCl	1:20:8 (molar ratio)
	($Al(C_3H_7O)_3$:i-PrOH:HCl):PVA	1:3 (weight ratio)

Table 3.4 Compositions of electrospinning solution #3

Solution A	TEOS:EtOH:H_2O:HCl	1:15:2:0.01 (molar ratio)
Solution B	$B(C_2H_5O)_3$:EtOH:HCl	1:15:8 (molar ratio)
	($B(C_2H_5O)_3$:EtOH:HCl): PVA	1:4 (weight ratio)
Solution C	$Al(C_3H_7O)_3$:i-PrOH:HCl	1:20:8 (molar ratio)
	($Al(C_3H_7O)_3$:i-PrOH:HCl):PVA	1:4 (weight ratio)

Our preliminary studies showed that slow gelation time is essential to produce uniformly spun fibers. A set of preliminary experiments showed that the pH value should be kept below 2 to produce fibers without beads. The uniformity of the fibers heavily depends on the surface properties of the droplet at the tip. The viscosity and/or the surface tension of the droplet depends on the mechanism of gelation. The pH value was adjusted by hydrochloric acid which catalyzes hydrolysis. In turn, it also controls the gelation mechanism. Since one of the electron donating alkoxy group ((OC_2H_5) of TEOS) was removed during hyrolysis, protonation of $HO\text{-}Si(OC_2H_5)_3$ species were not favorable and therefore, the other hydrolysis and condensation reaction rates become relatively slower resulting in long gelation time and weakly branched structure, which has advantageous to spinning process. In order to obtain sufficiently linear backbone the branchings must be minimized. This can be achieved by partial hydrolysis of TEOS. Therefore, H_2O/TEOS molar ratio was taken as 2 in our researh.

It was not easy to prepare Solution B and C, because aluminum isopropoxide and triethyl borate were extremely reactive and their fast gelation prevented the formation of alumina borosilicate mixture. Therefore, in order to obtain the transparent solutions of B and C, PVA first was mixed with excess amount of HCl, and then with the parent alcohol of each alkoxide, and finally the proper alkoxide was added to this solution. The three solutions of alkoxides thus prepared were then mixed to make the final solution for electrospinning. The PVA separately added at the beginning delayed the diffusion of molecules and thus retarded immature gelation.

3.4 Electrospinning

The setup consisting of a DC voltage power supply (Gamma High Voltage Research Inc., Model ES30-20W), a plastic capillary tube, and a metal collector was typically operated in air. The alumina borosilicate/PVA composite solution was contained in a plastic capillary. A copper pin connected to a high-voltage generator was placed in the solution and it was kept in the capillary by adjusting the angle between capillary and the fixing bar. A grounded iron drum, covered with an aluminum foil served as the counter electrode. The distance between the capillary tip and the collector was measured. A high voltage was applied to the solution and a dense web of alumina borosilicate/PVA composite fibers were collected on the aluminum foil.

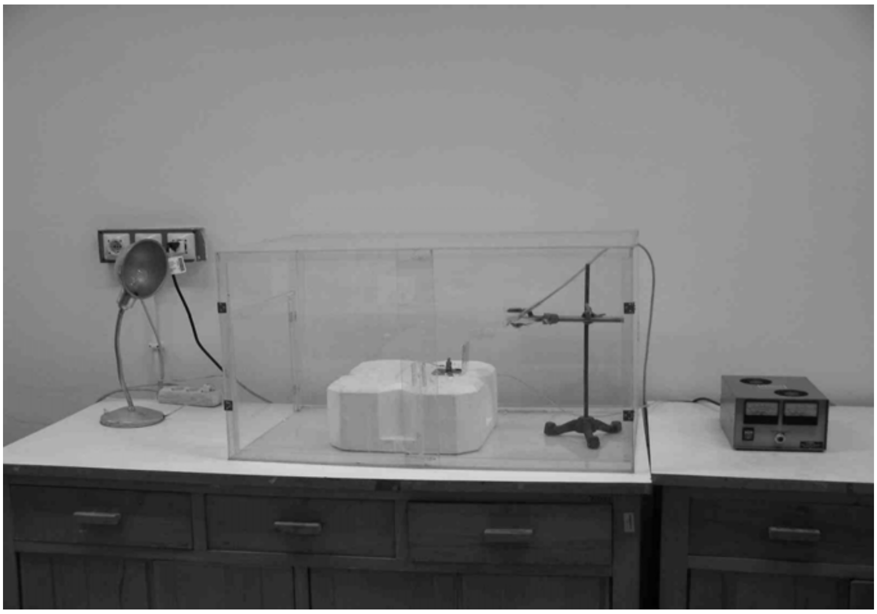

Figure 3.2 Electrospinning System

3.5 Heat Treatment

Alumina borosilicate/PVA nanofibers were dried for 6 hours at 70°C under vacuum, then sintered in a tubular high-temperature furnace for about 2 hours at 800, 1000, and 1200°C under atmospheric conditions. After heat treatment volatile and organic groups were removed and pure alumina borosilicate nanofibers remained.

3.6 Parameters Examined

During electrospinning, some problems such as high fiber diameter, discontinuity of the spinning process, bead formation on the fibers, and surface defects were encountered. To solve these problems, some parametric studies, which are (i) applied electric voltage, (ii) tip-to-collector distance, and (iii) viscosity were performed.

3.7 Chemical Characterization

3.7.1 Fourier Transform Infrared (FTIR) Spectroscopy

The FTIR spectra of alumina borosilicate nanofibers were recorded at room temperature with a Bruker IFS 66/S instrument in the wavenumber range from 400 to 4000 cm^{-1}. The samples were prepared in the form of thin pellets using KBr.

3.7.2 Scanning Electron Microscopy (SEM)

For the scanning electron microscopy (SEM), JSM-6400 Electron Microscope (JEOL), equipped with NORAN System 6 X-ray

Microanalysis System & Semafore Digitizer (Metallurgical Engineering Department, METU) was used. For the SEM characterization the samples were coated with a very thin layer of a gold-palladium (Au-Pd) alloy in order to have SEM images.

3.7.3 X-Ray Diffraction (XRD)

The crystallographic orientation of alumina borosilicate nanofibers was examined by means of a Philips PW1140/00 diffractometer by using CuKα radiation (λ = 1.542A°) witha Ni filter (Physics Engineering Department, Hacettepe University).

3.7.4 Differential Thermal and Thermogravimetric Analysis (DTA/TG)

Combined Differential Thermal Analysis (DTA) and Thermogravimetric Analysis (TG) were carried out between 25 and 1300°C using a Rigaku 2.22E2 type instrument (Mining Engineering Department, Hacettepe University) for determining the mass and thermal changes accompanying solvent/volatile removal, decomposition and crystallization processes. The DTA/TG curves were obtained simultaneously for each sample in the temperature range of 20-1300 °C, at a heating rate of 10K/min.

CHAPTER 4

RESULTS AND DISCUSSION

The results of the performed experiments will be discussed in this chapter. This part includes results from preliminary experiments, SEM, FT-IR, DTA/TGA, and XRD analyses carried out throughout the study.

4.1 Preliminary Experimental Results

As mentioned in the previous chapter, aluminum ethoxide as aluminum source and toluene as solvent were used instead of aluminum isopropoxide and its parent alcohol isopropyl alcohol at the initial stages of this study. Figure 4.1 shows SEM micrographs of these electrospun alumina borosilicate/PVA composites prepared at different electric voltages, with different tip-to-target distances. As it is seen from the images, fibers could not be formed efficiently. Moreover, beaded thick fibers, and some interesting branched structures were observed.

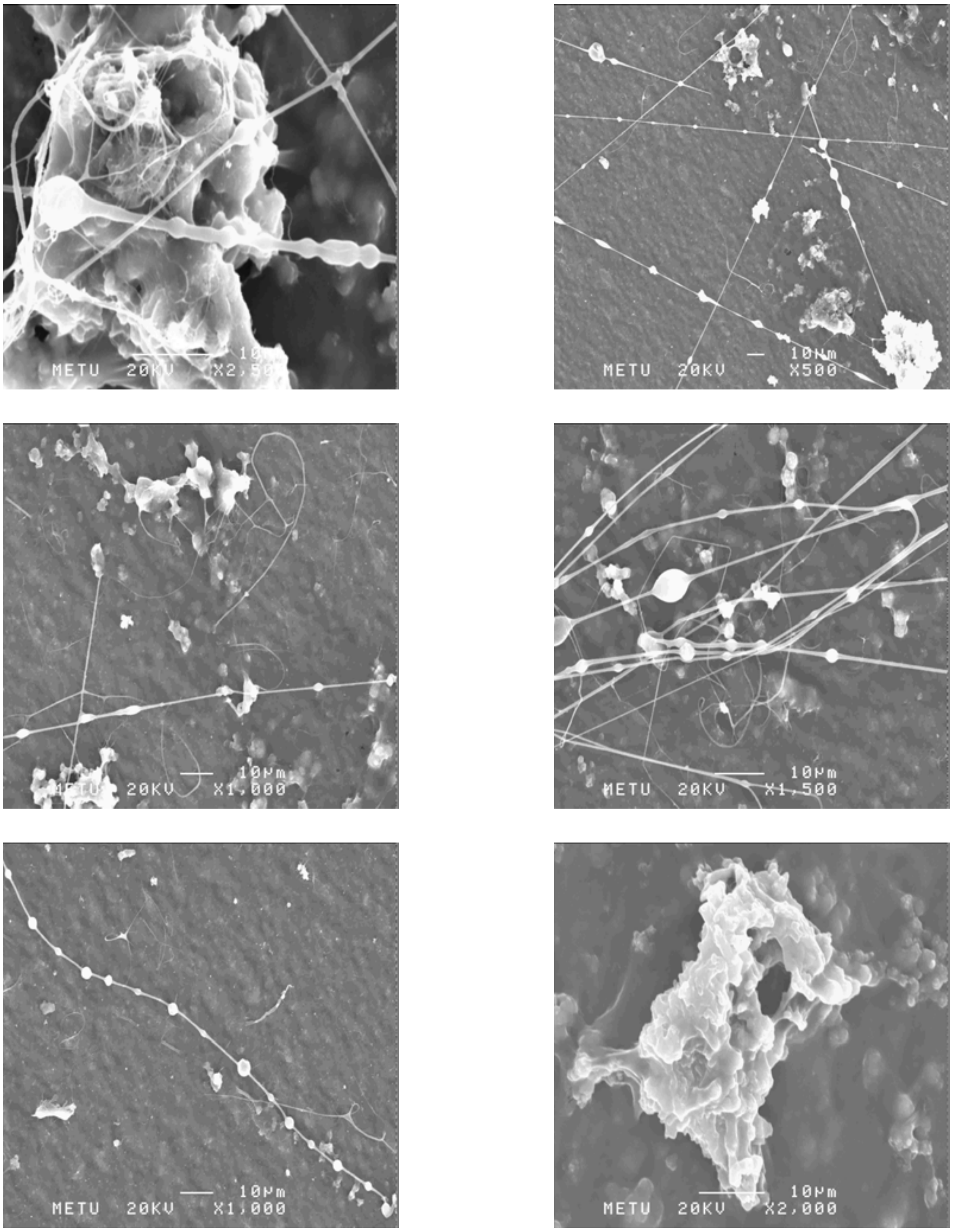

Figure 4.1 SEM micrographs of aluminum borosilicate/PVA electrospun fibers prepared by using aluminum ethoxide as a metal precursor and toluene as a solvent.

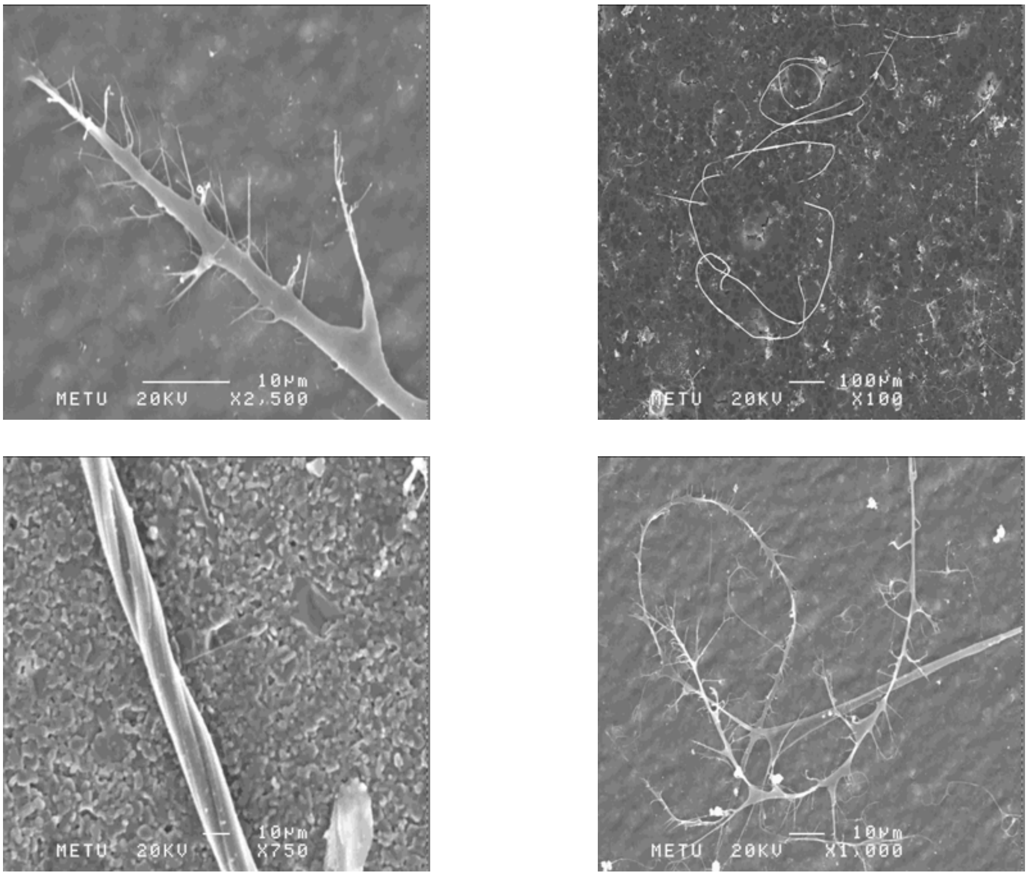

Figure 4.1 (contd') SEM micrographs of aluminum borosilicate/PVA electrospun fibers prepared by using aluminum ethoxide as a metal precursor and toluene as a solvent.

Due to the poor fiber quality in the initial experiments, aluminum isopropoxide and isopropyl alcohol were used instead of aluminum ethoxide and toluene. Aluminum isopropoxide was preferred because it had bigger alkyl group than aluminum ethoxide providing steric hindrance which delays and controls gelation. As solvent isopropyl alcohol was used because it was a polar protic solvent. Hence it stabilized the reactants due to its polarity, and also solvated and deactivated the nucleophile through hydrogen bonding interactions, which decreased the reaction rate and increased the gelation time.

Oppositely toluene was a non-polar aprotic solvent. It could not stabilize the reactants and could not solvate the nucleophile, and therefore the reactants remain highly reactive. So when toluene was used the gelation time came out to be much faster than that of isopropyl alcohol [57].

Thus, by using aluminum isopropoxide and isopropyl alcohol, a reduction in the reaction time was observed and more homogeneous alumina borosilicate/PVA solution was obtained. This solution could be electrospun easier than the materials used in the first case. Therefore, the rest of the study is based on these materials. However, there were still some problems in the fiber and process characteristics such as fiber diameter, discontinuity of the spinning process, bead formation, surface defects (ribbon-like and pretzel-like structures). The typical micrographs of these fibers are shown in Figure 4.2. To solve these problems, some parametric studies have been performed. They will be explained in section 4.2.

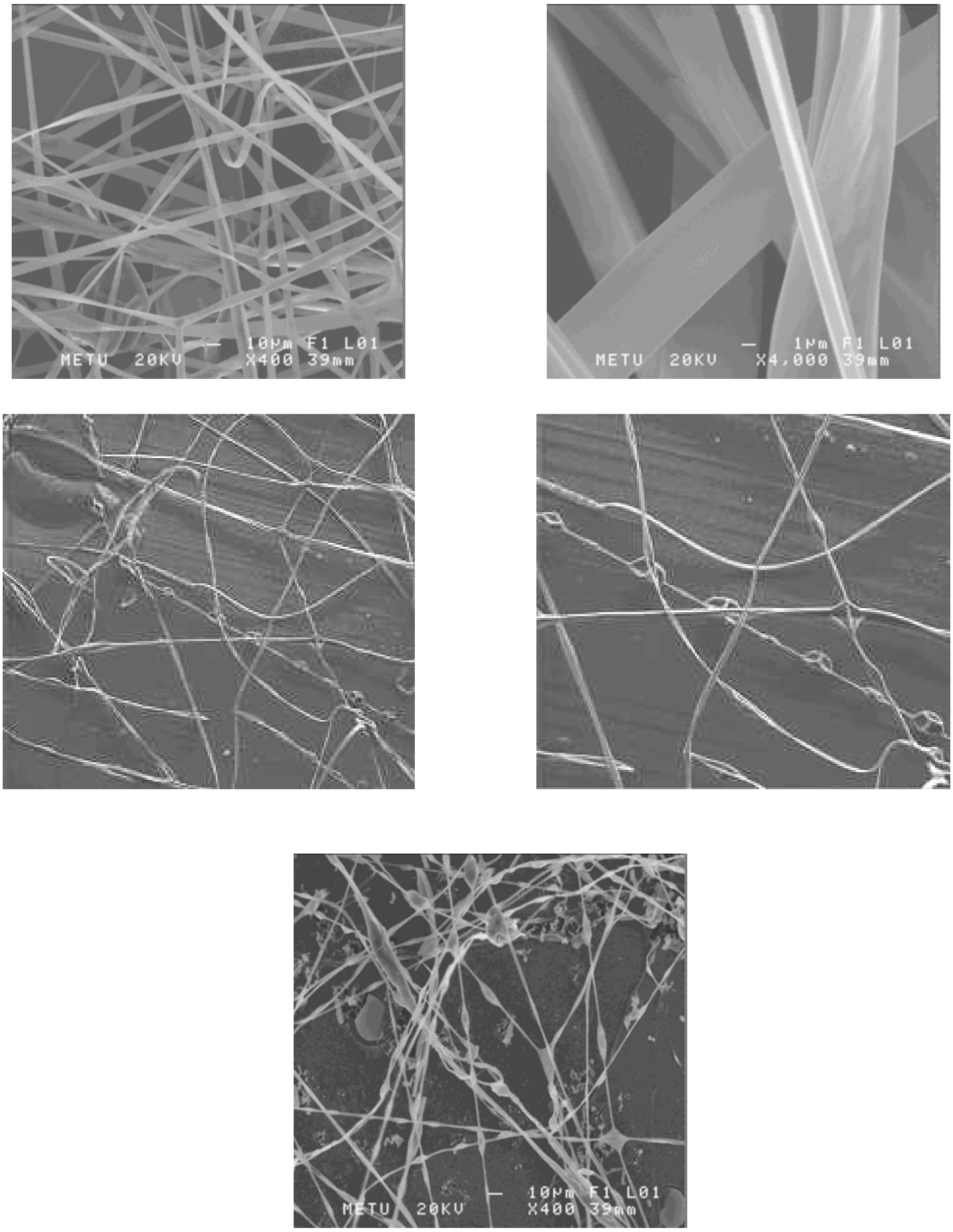

Figure 4.2 SEM micrographs of aluminum borosilicate/PVA fibers prepared by using aluminum isopropoxide as a metal precursor and isopropyl alcohol as a solvent.

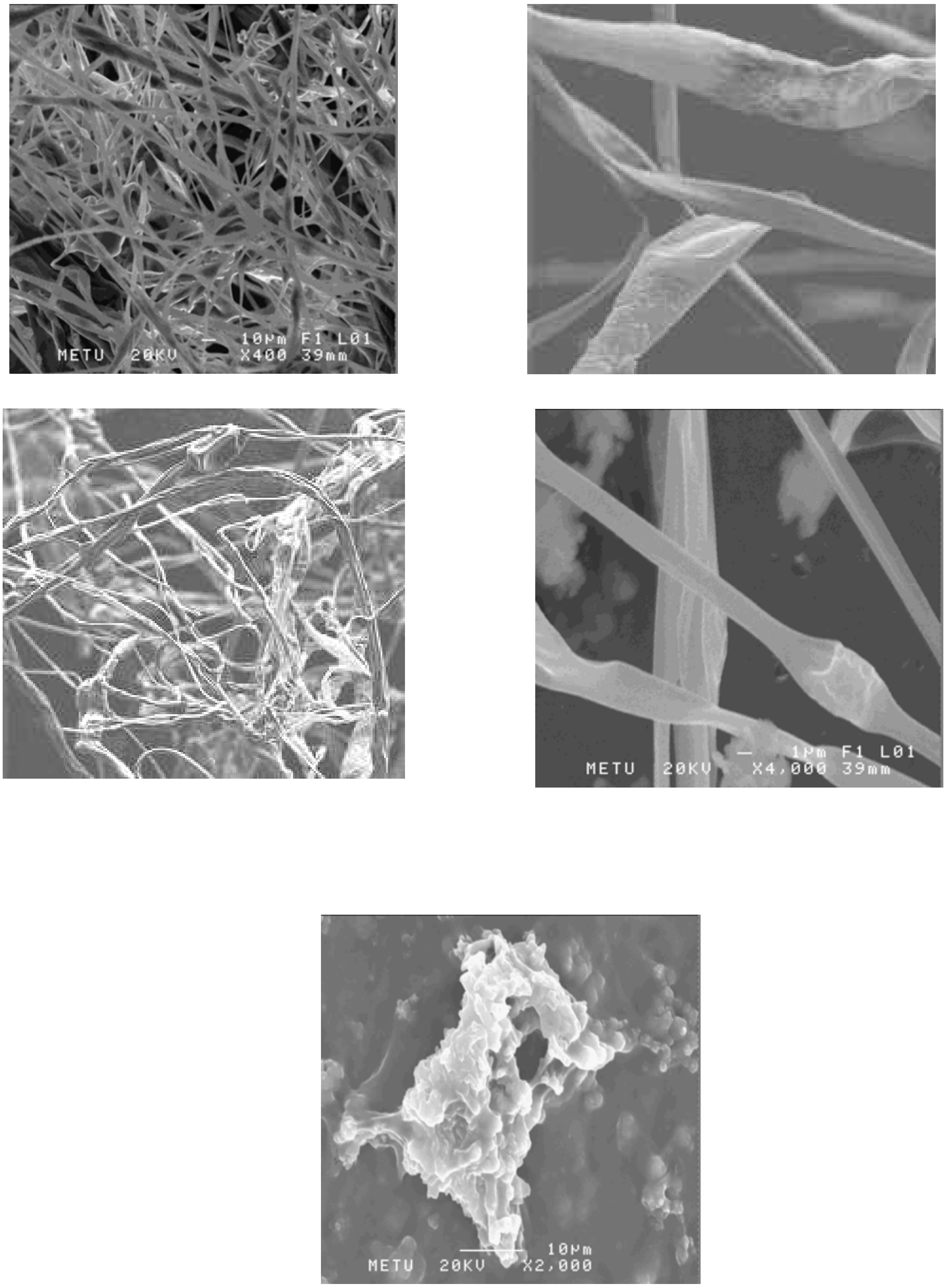

Figure 4.2 (contd') SEM micrographs of aluminum borosilicate/PVA fibers prepared by using aluminum isopropoxide as a metal precursor and isopropyl alcohol as a solvent.

4.2 Parametric Studies

During the experimental studies, it was difficult to maintain stable solution properties and electrospinning conditions. Thus, some parametric considerations were applied to obtain favorable nanofibers. These were (i) viscosity by using different fractions of solvents and PVA, (ii) changing applied electric voltage, and (ii) tip-to-collector distance

4.2.1 Effects of Viscosity and Solvent

Solution viscosity was a very important parameter in successful electrospinning. As it was mention before, in this study, three different solutions were tried to get fine nanofibers. Their viscosity values are shown in Table 4.1.

Table 4.1 Viscosities of three different electrospinning solutions

Electrospinning Solution #	Viscosity (poise)
1	2.42
2	6.5
3	4.6

Presence of beads in electrospun fibers was a crucial problem. As shown in Figure 4.3, beaded and defective nanofibers formed when the viscosity was 2.42 poise (Solution 1). When the viscosity of the same solution increased to 6.5 poise (Solution 2) by the addition of

PVA, bead formation decreased dramatically as seen from Figure 4.4. However, this time, the physical gelation at the tip of the capillary clearly obstructed the continuity of the process. That's why; the alcohol concentration was increased to delay the gelation time of the solution, but by keeping the viscosity sufficiently high. The viscosity was about 4.6 poise (Solution 3). Finally bead-free and thin alumina-borosilicate/PVA nanofibers were obtained as seen from Figure 4.5. From this, all studies were done with using Solution 3.

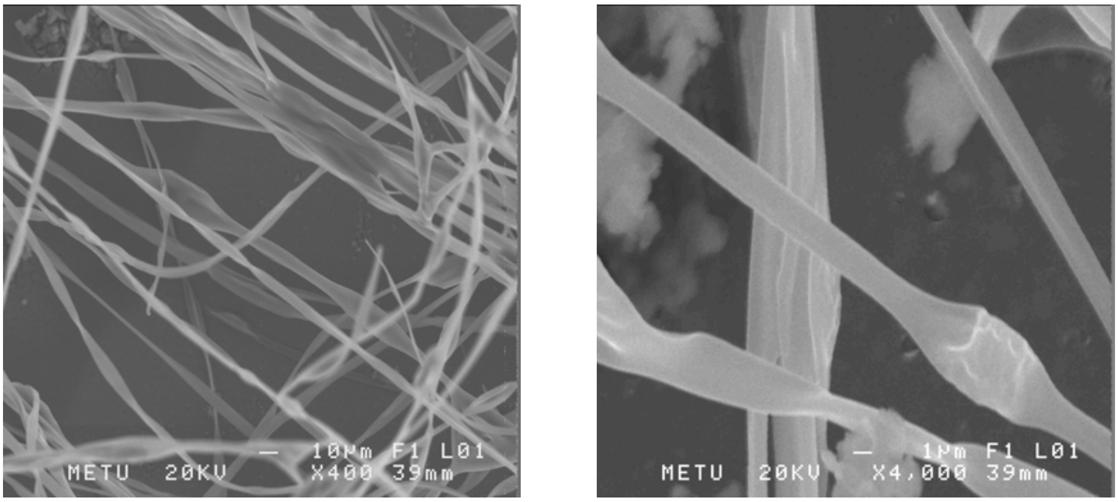

Figure 4.3 SEM micrographs of PVA/alumina borosilicate fibers electrospun from solution with viscosity of 2.42 poise (Electrospinning solution #1)

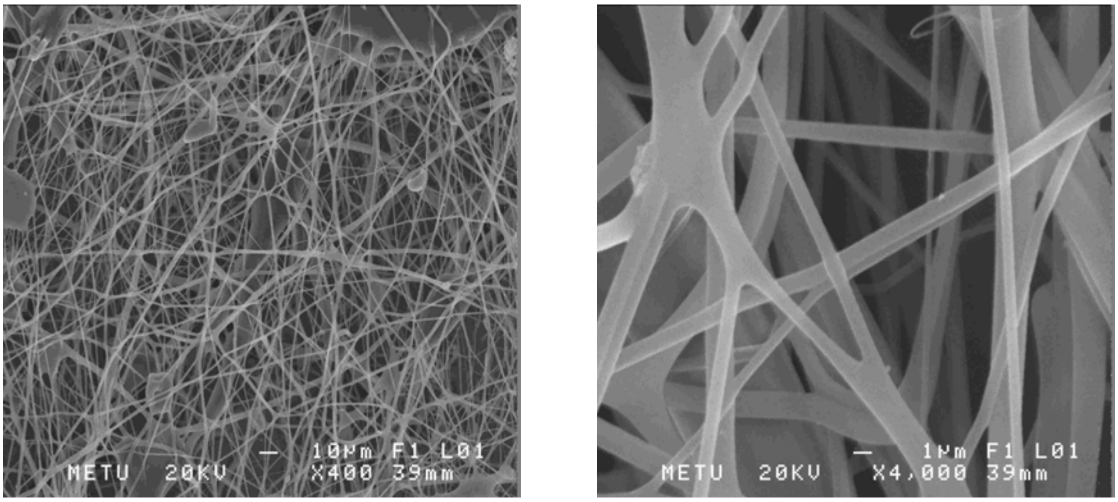

Figure 4.4 SEM micrographs of PVA/alumina borosilicate fibers electrospun from solution with viscosity of 6.5 poise (Electrospinning solution #2)

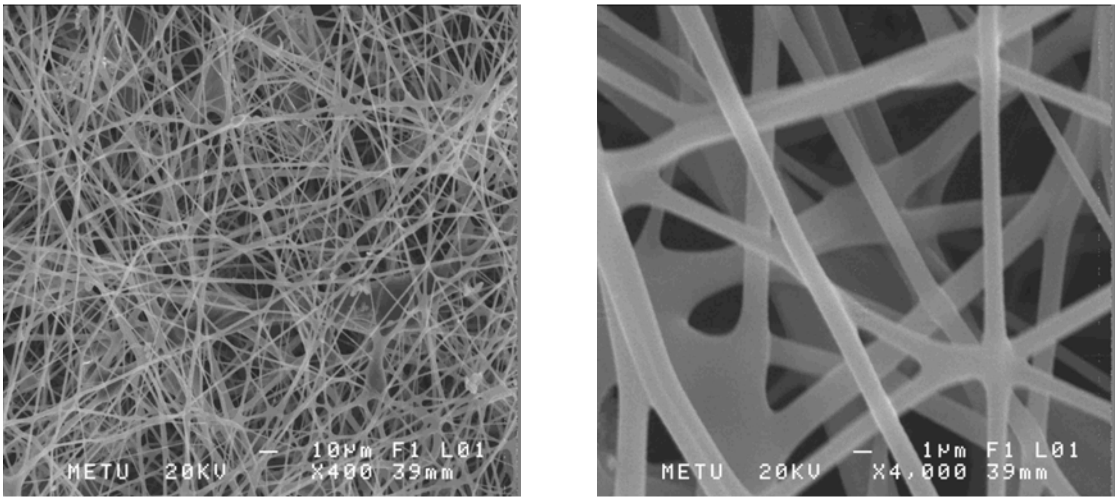

Figure 4.5 SEM micrographs of PVA/alumina borosilicate fibers electrospun from solution with viscosity of 4.6 poise (Electrospinning solution #3)

4.2.2 Effect of Applied Electric Voltage

The electrospun specimens were analyzed to see the effect of electrical voltage on the diameter of the fibers formed. Figure 4.6(a-b) shows the average fiber diameters for electric voltages of 8 kV, 10 kV, 12 kV, and 15 kV respectively at a distance of 15 cm. By changing the electric voltage the surface charges that affected the stability and production of nanofibers increased, thus smaller fiber diameters were obtained as shown in Table 4.2.

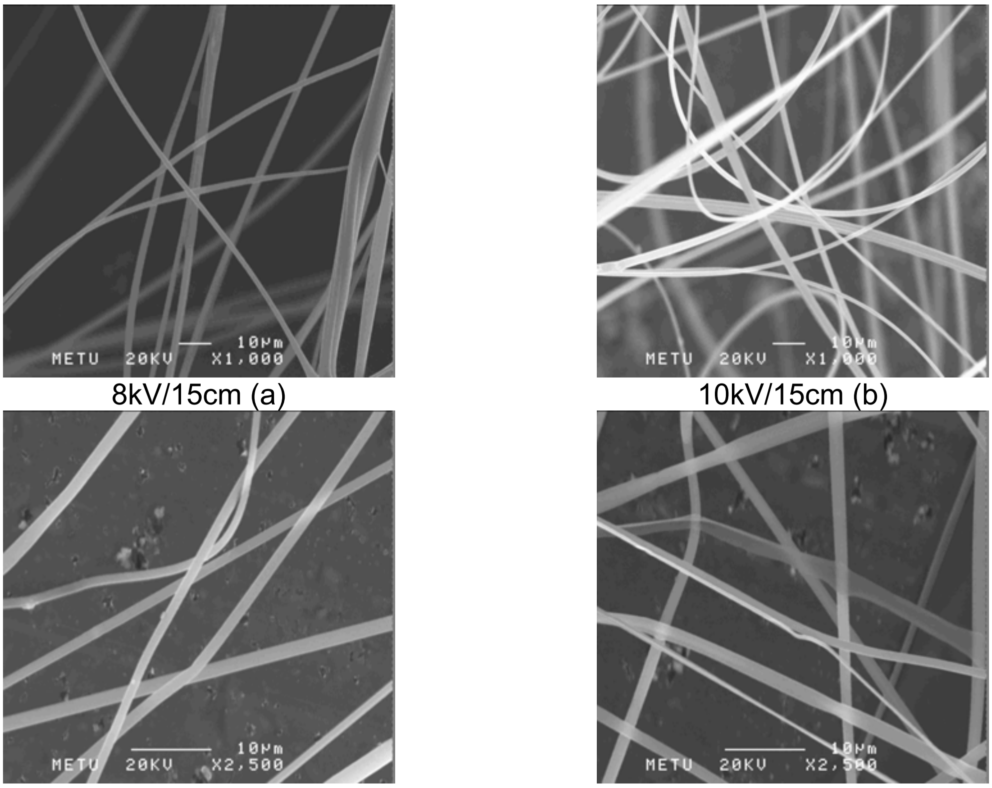

8kV/15cm (a)

10kV/15cm (b)

12kV/15cm (c)

15kV/15cm (d)

Figure 4.6 SEM micrographs of PVA/alumina borosilicate fibers electrospun at 15cm tip-to-collector distance and various electric voltages: (a) 8 kV; (b) 10 kV; (c) 12 kV; (d) 15 kV.

The standard deviation of diameters was also determined from 10-20 samples depending on the number of availability from SEM picture.

Table 4.2 Fibers diameters of various sample electrospun at 8, 10, 12, and 15kV applied electric voltage.

Applied electric voltage	Average fiber diameter (nm)	Standard deviation (nm)	Maximum Fiber diameter (nm)	Minimum Fiber diameter (nm)
8 kV	2226	407	3170	1854
10 kV	2012	676	3073	1170
12 kV	1290	368	2087	854
15 kV	871	183	1204	656

4.2.3 Effect of Tip-to-Collector Distance

The effect of tip-to-collector distance on the fiber diameter was examined. In Figure 4.7(a-c), alumina borosilicate/PVA fibers electrospun distances ranging from 7cm to 15 cm at a constant electric voltage of 10kV are shown.

Table 4.3 Fibers diameters of various sample electrospun at 7, 10, and 15cm tip-to-collector distance.

Tip-to-collector distance	Average fiber diameter (nm)	Standard deviation (nm)	Maximum Fiber diameter (nm)	Minimum Fiber diameter (nm)
7 cm	1270	631	2620	750
10 cm	1233	426	2100	700
15 cm	871	183	1204	656

It was observed that the fiber diameters decreased with increasing tip-to-collector distance as shown in Table 4.3.

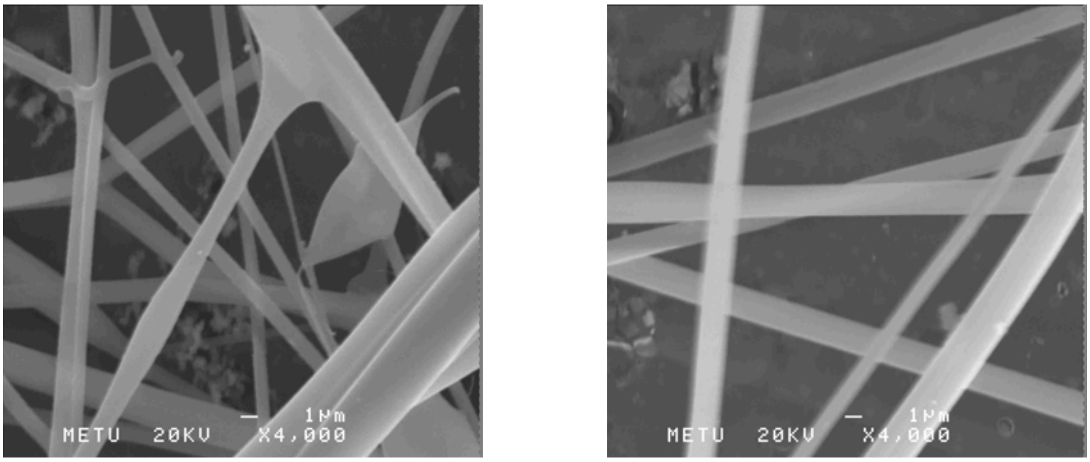

10 kV/7cm (a) 10 kV/10cm (b)

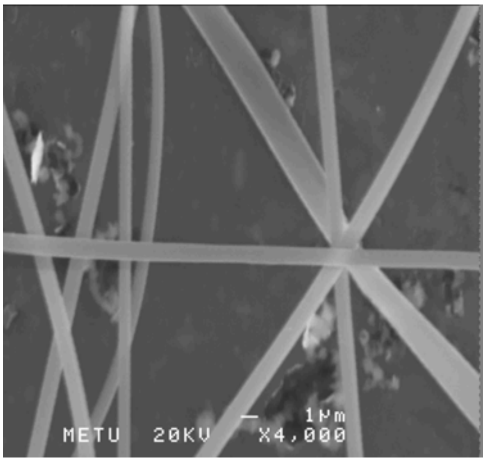

10 kV/15cm (c)

Figure 4.7 SEM micrographs of PVA/alumina borosilicate fibers electrospun at 10kV electric voltage and various tip-to-collector distances: (a) 7cm; (b) 10 cm; (c) 15cm.

4.3 Sintering Effects

SEM micrographs showing alumina borosilicate/PVA fibers electrospun at 15kV and 15 cm are given in Figure 4.8 The diameter distribution of the alumina borosilicate/PVA fibers dried at 70°C (Figure 4.9a) ranges from 650 nm to 1200 nm and the majority are in the range of 750–950 nm. The average diameter is 871 nm with a standard deviation of 183 nm. In order to obtain pure and dense alumina borosilicate fibers, the electrospun fibers were sintered at temperature of 800°C. Due to the removal of organic contents from the fiber surface, the diameter distribution of the alumina borosilicate fibers (Figure 4.9b) ranges from 150 nm to 650 nm and the majority are in the range of 250–550 nm. The average diameter is 404 nm with a standard deviation of 129 nm. These alumina borosilicate fibers are shown in Figure 4.10. Besides, these fibers were sintered at 1000°C and 1200°C. At 1000°C, the fiber structure has disappeared and smooth surface is observed by the linkage of fibers as shown in Figure 4.11, the fiber structure is still absent and structure can be characterized by short discontinuous entities with sharp edges. Such structures may be originated from the agglomeration and sintering of fibers at high temperatures. In some cases upon high temperature sintering (at 1200°C), large sized and rough surfaced fibers are observed. Some morphological changes are also expected upon the formation of new compounds in crystalline form at even higher temperatures as shown in Figure 4.12. This idea is also supported by the XRD analyses.

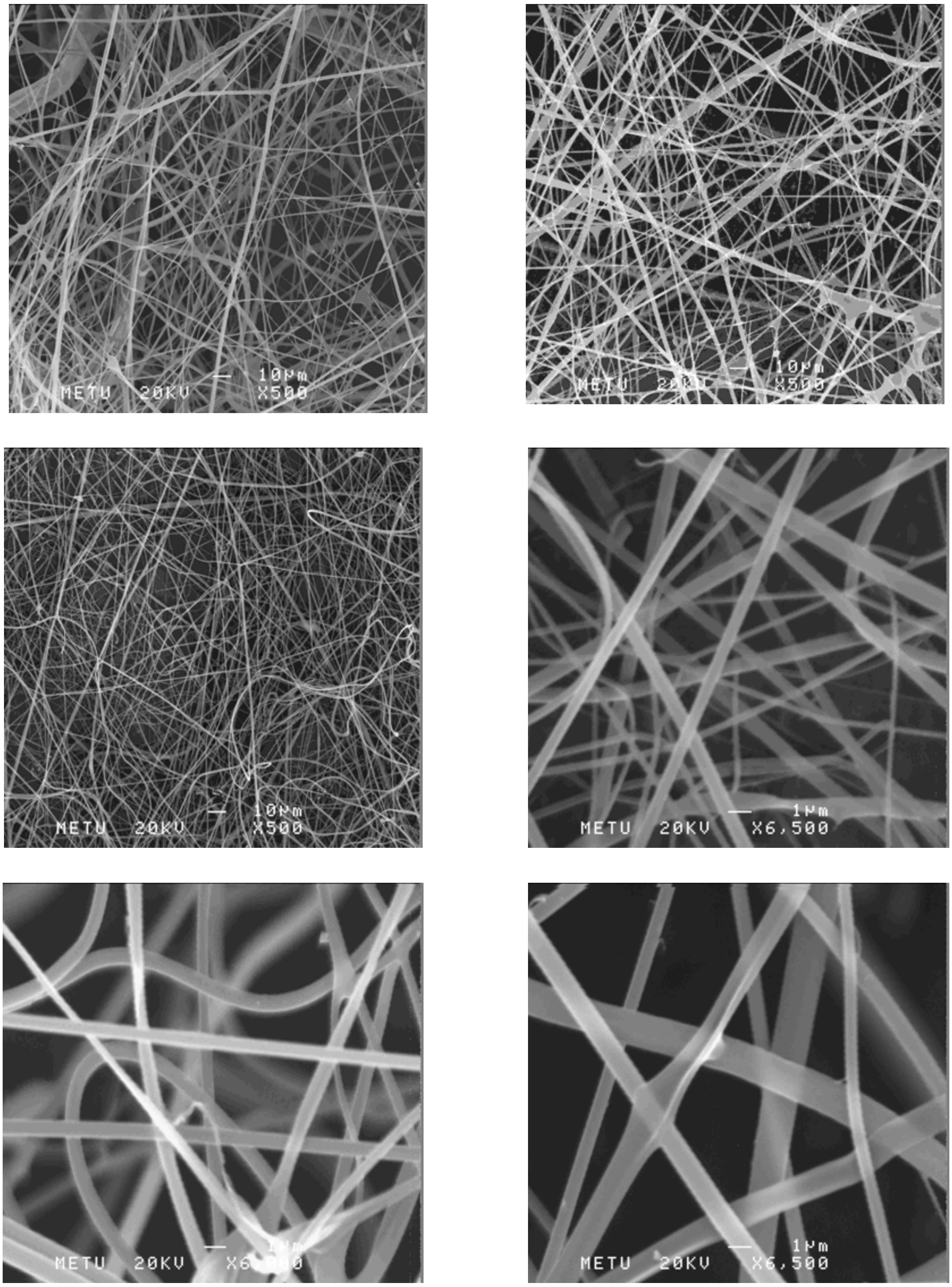

Figure 4.8 SEM micrographs of alumina borosilicate/PVA composite fibers.

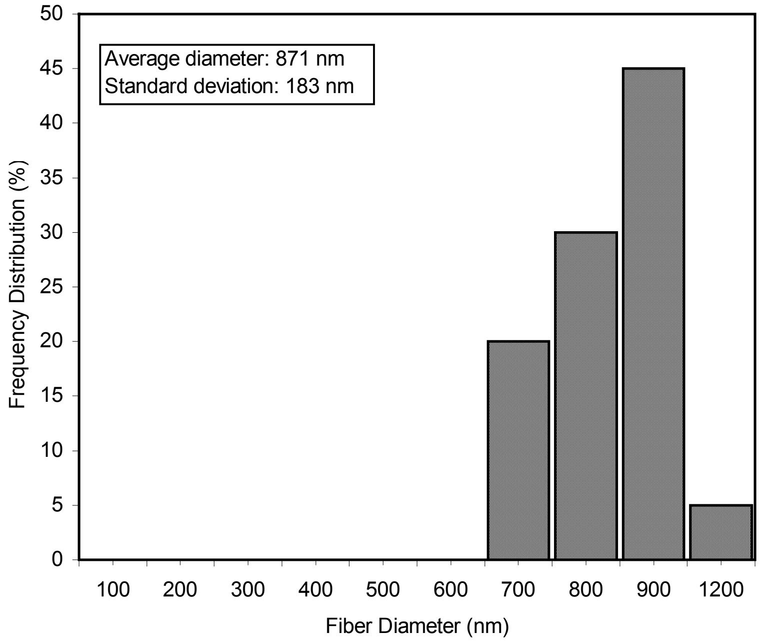

(a)

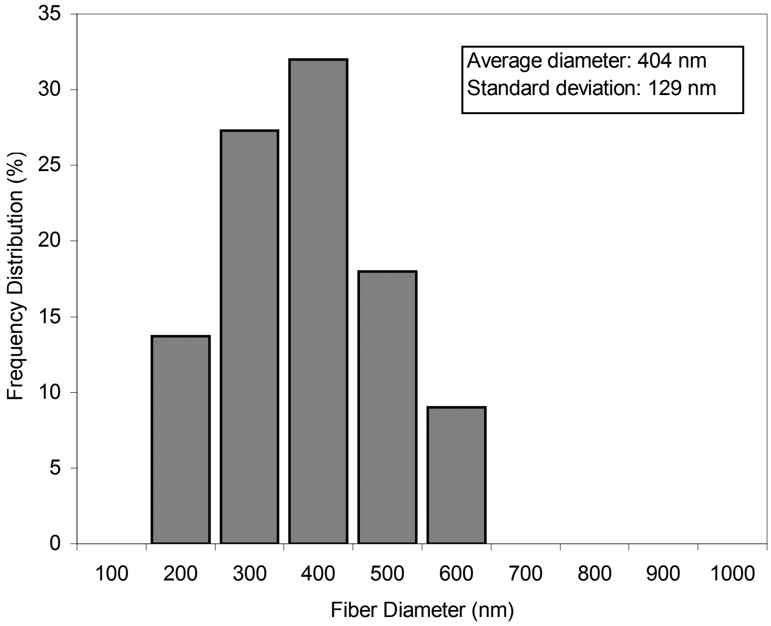

(b)

Figure 4.9 Frequency distribution for fibers: (a) dried at 70°C (b) sintered at 800°C.

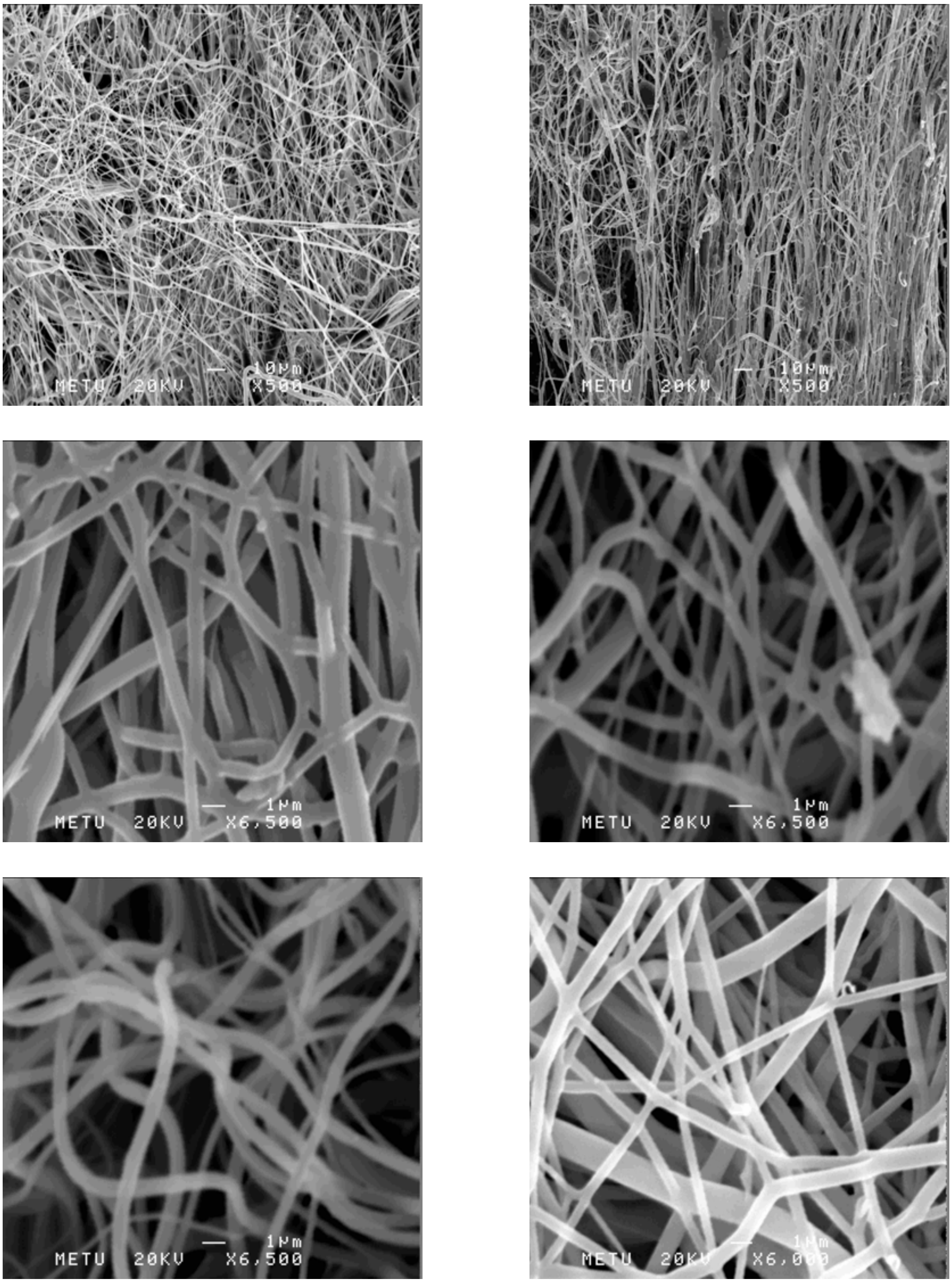

Figure 4.10 SEM micrographs of alumina borosilicate fibers sintered at 800°C

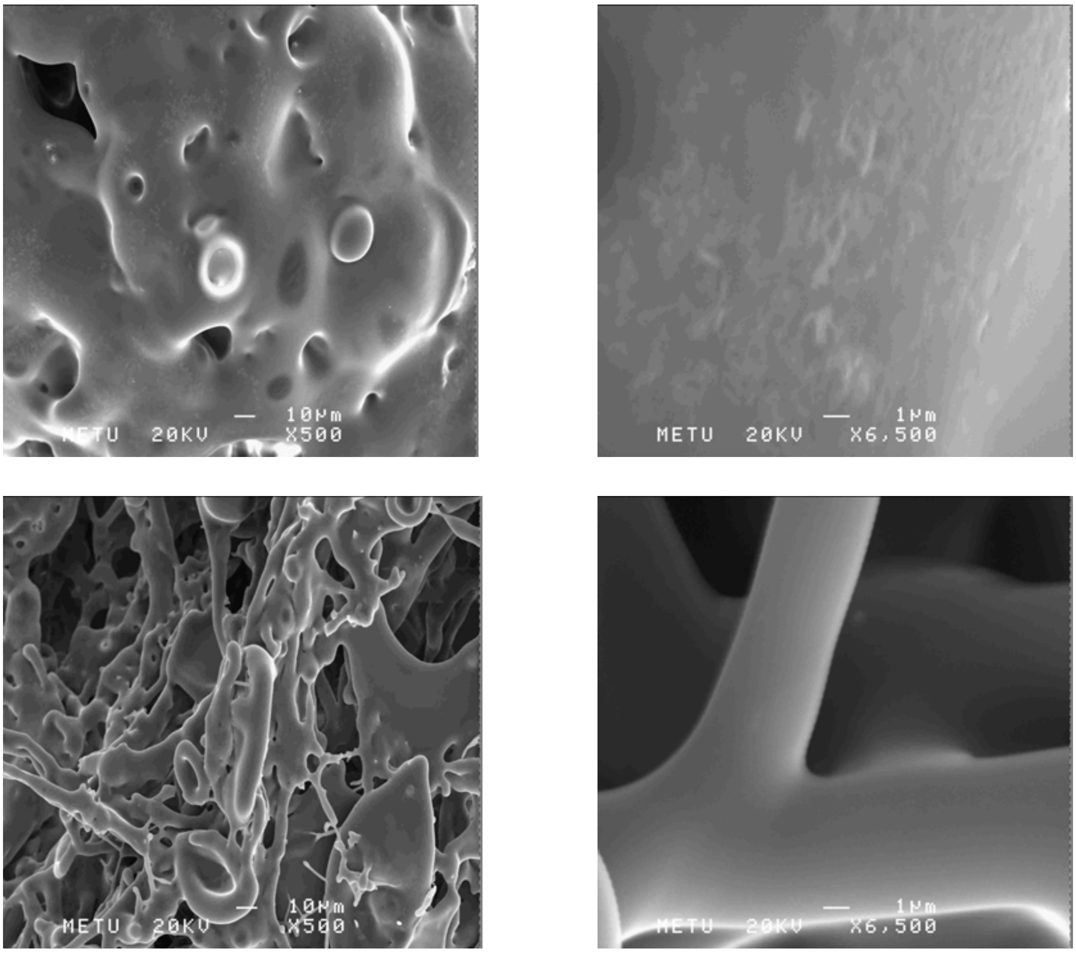

Figure 4.11 SEM micrographs of alumina-borosilicate fibers sintered at 1000°C

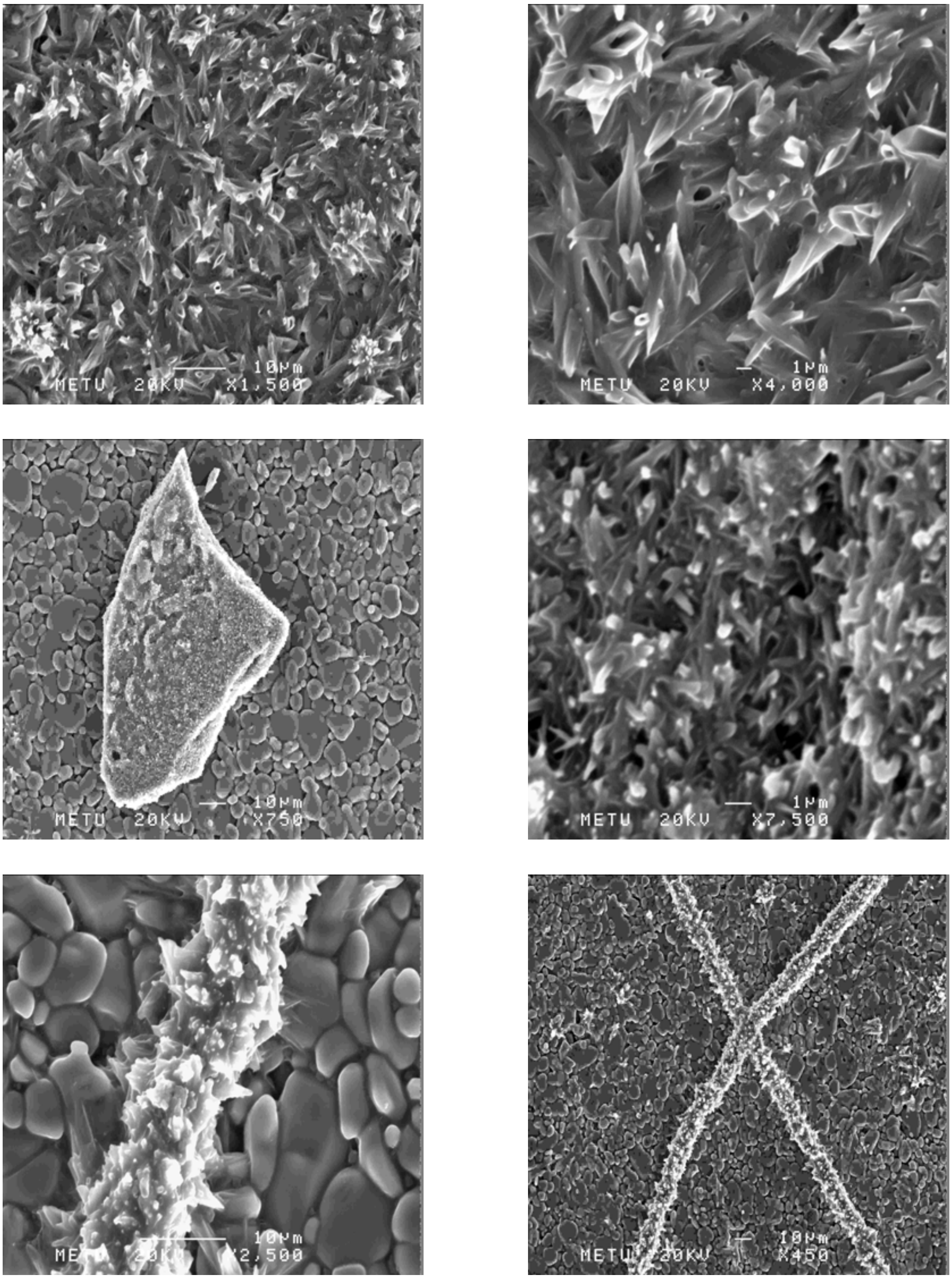

Figure 4.12 SEM micrographs of alumina borosilicate fibers sintered at 1200°C

4.4 Fourier Transform Infrared (FT-IR)

Figure 4.13 shows the FT-IR spectra the PVA/alumina borosilicate fibers at room temperature, and for those sintered at temperatures of 800°C and 1000°C. In Figure 4.13(a), the alumina borosilicate/PVA fibers show a broad peak at 3429 cm−1 corresponding to H–OH stretch; and the characteristic absorption peaks at about 2929, 1650, 1557, 1084, 945, 792 and 578 corresponding to vibration bands of C−H, C−C, C−O, O−H, respectively [67]. After sintering, between 800°C and 1000°C, all these peaks coming from water and organic species disappeared. In addition, at these temperatures, a group of clear new peaks, which may be attributed to the formation of crystalline inorganic phase, appears at 400-1600 cm^{-1}. The absorption peaks in Figure 4.13(b) are found at $1406cm^{-1}$ (B-O-Sİ band)[68], $1094cm^{-1}$ (Si-O-Si band) [69], $912cm^{-1}$ (B-O-Si band) [70], $800cm^{-1}$ (Si-O-Si bending band) [70], $675cm^{-1}$ (B-O-Si band) [68], $455cm^{-1}$ (Si-O-Si or Al-O-Si bending band) [72]. The absorption bands around $1050cm^{-1}$ attributed to Al-O-Si bonds [73] cannot be observed. Thus, it may be admitted that these peaks overlapped each other. When the fiber was sintered at 1000°C a new peak appeared at 606 cm^{-1}, which may be assigned to Al–O stretch band of AlO_6 (Figure 4.13(c)) [74].

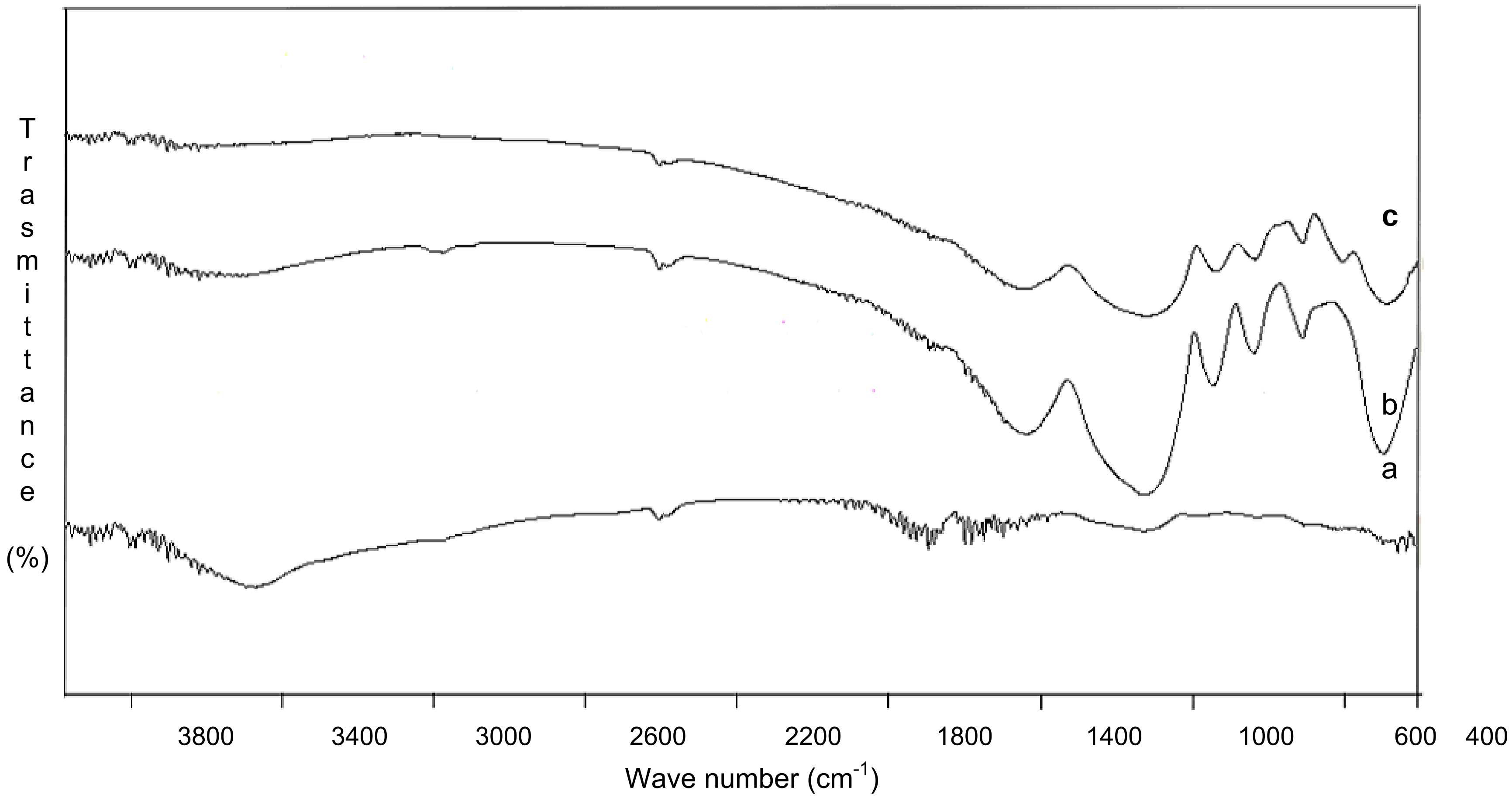

Figure 4.13 FT-IR spectra of various fiber samples: (a) As-dried at 70°C alumina-borosilicate/PVA composite fibers; (b) sintered at 800°C; (c) sintered at 1000°C

4.5 X-Ray Diffraction (XRD)

The XRD patterns of the various fiber samples, the PVA/alumina borosilicate fibers and for those sintered at temperatures of 800°C and 1000°C were analyzed. It was observed that the position of these diffraction peaks didn’t change at 800°C and 1000°C. As shown in Figure 4.14(a), a broad peak appeared around $2\theta = 20°$, corresponding to the (101) plane of semicrystalline PVA [75] in the XRD curve of alumina borosilicate/PVA composite fiber. This peak showed that the crystallinity of PVA is largely influenced by the presence of alumina borosilicate inorganic species. After sintering at 800°C (Figure 4.14(b)), it was observed that the crystalline peak disappeared due to the decomposition PVA and also new shaped peaks appeared. These peaks belong to mainly mullite ($Al_6Si_2O_{13}$) crystals, and also to $Al_4B_2O_9$ crystals [76]. Also, there is a broad band around $2\theta=22°$ which is characteristic of vitreous SiO_2 [77]. At 1000°C, the crystallization of vitreous SiO_2 phase occurred. The XRD peak around 22° (Figure 4.14(c)) was assigned to a type of crystalline SiO_2, cristobalite [78]. In addition, some new diffraction peaks appeared indicating the formation of $Al_4B_2O_9$ and $Al_{18}B_4O_{33}$ crystals in which $Al_{18}B_4O_{33}$ was predominant [76].

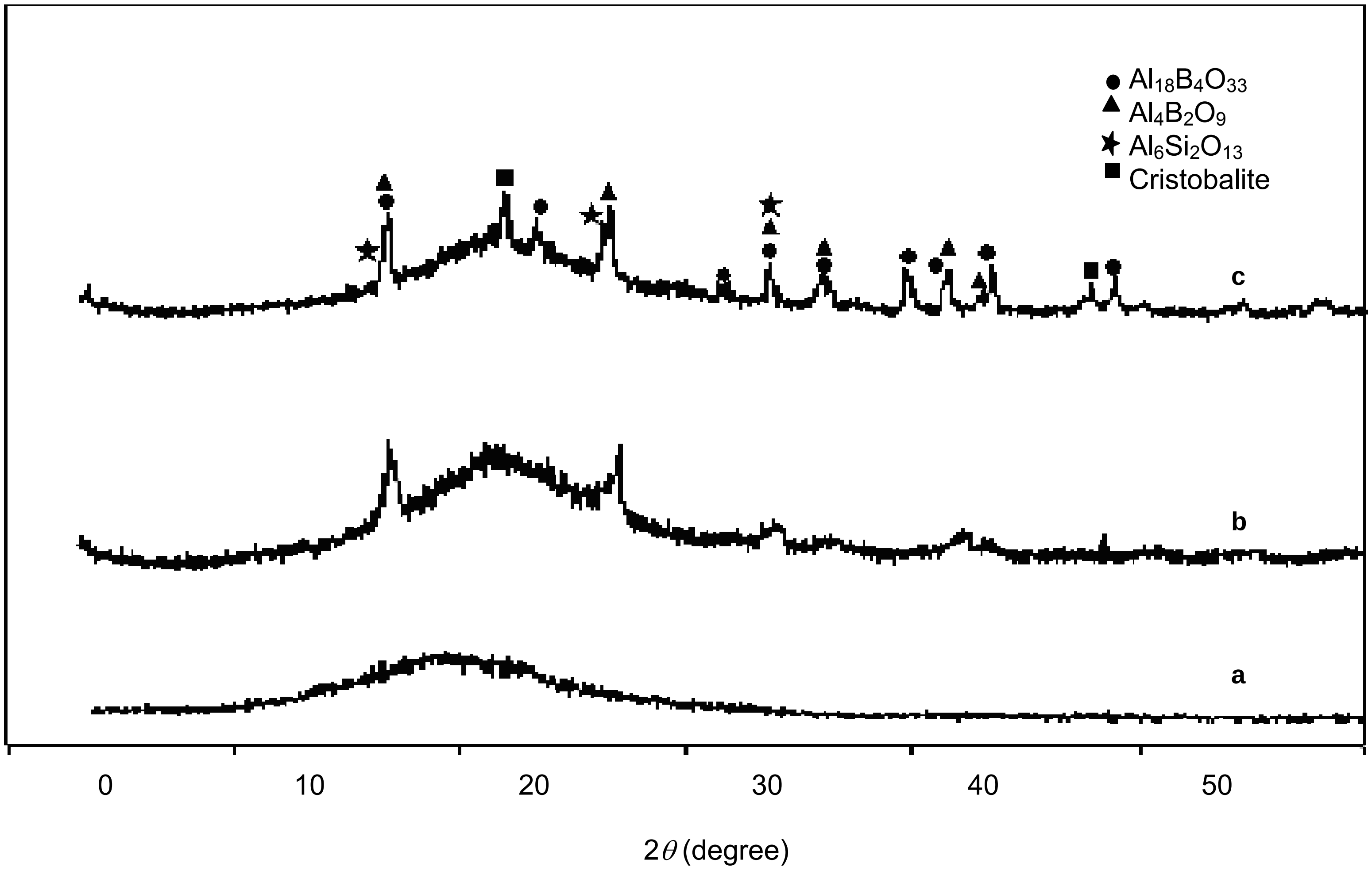

Figure 4.14 XRD results of various fiber samples: (a) As-dried at 70°C alumina-borosilicate/PVA composite fibers; (b) sintered at 800°C; (c) sintered at 1000°C

4.6 Differential Thermal and Thermogravimetric Analysis (DTA/TG)

The results of simultaneous TG and DTA analyses of fibers are shown in the Figure 4.15. As observed in the DTA curve, there were three endothermic peaks around 130, 192 and 205°C corresponding to the loss of absorbed water, decomposition of remaining alkyl groups, and the pyrolysis of PVA by a dehydration on the polymer side chain [79]. Moreover, the weight loss of the sample was observed with the TG curve as about 80%. The exothermic peaks at about 420, 440, 462 and 550°C in the DTA curve were thought to be due to the continue decomposition of the main chain of PVA [80]. There was only a weight loss of 7.3% from 400°C up to a temperature of 700°C. There is no further weight loss above the temperature of 700°C, which indicates the formation of pure inorganic oxide in crystalline form.

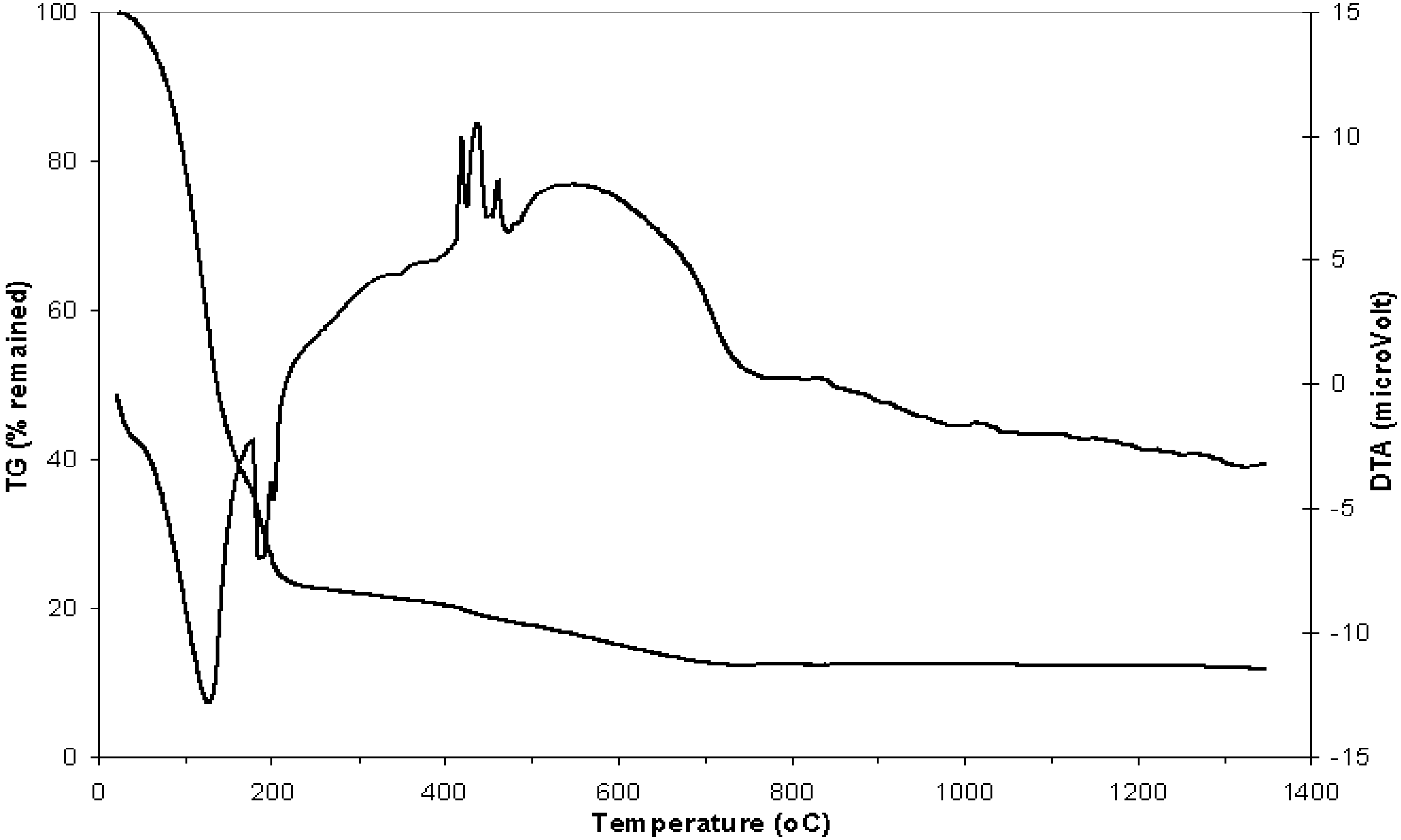

Figure 4.15 TG-DTA curves of precusor fibers of alumina borosilicate/PVA fibers

CHAPTER 5

CONCLUSIONS

1. Alumina borosilicate/PVA fibers were prepared by the sol-gel method and electrospinning technique for the first time in this study.

2. Alumina borosilicate nanofibers, with diameters down to 150nm, were prepared through high temperature sintering treatment.

3. The increase in the applied electric voltage decreased fiber diameter as also observed in the literature [42].

4. A dependence of fiber diameter to tip-to-collector distance was also observed. An increase of the tip-to-collector distance reduced the diameter of the fibers.

5. Increasing the viscosity of the solution decreased bead formation in electrospinning. The high viscosity eliminated the bead formation as also noted in literature.

6. Aluminum isopropoxide was used as aluminum source instead of aluminum ethoxide due to it has bigger alkyl group.

It leads to a decrease in the reaction rate and thus to an increase in gelation time.

7. Aluminum isopropyl alcohol, which is a polar protic solvent, was used instead of toluene, which is non-polar aprotic solvent. In this manner, it was observed that the gelation time increased, and more uniform fibers were obtained.

8. The alcohol concentration in the electrospinning solution was also important to prevent fast gelation problem. Alcohol retards gelation.

9. The XRD spectra showed that $Al_6Si_2O_{13}$ and $Al_4B_2O_9$ crystals, and vitreous silica formed around 800^oC.

10. When the sintering temperature was increased to 1000^oC cristobalite and new $Al_{18}B_4O_{33}$ crystals were observed.

RECOMMENDATIONS

- By making further modifications on the parameters of sol-gel and electrospinning processes, uniform alumina borosilicate nanofibers with smaller diameter could be formed.

- Different metal alkoxides, which hydrolyse slowly, should be tried in order to avoid fast gelation.

- Mechanical, electrical or chemical characterization should be carried out for this ceramic material to explore its potential industrial applications.

REFERENCES

1. Richard Feynman *There's Plenty of Room at the Bottom.* An Invitation to Enter a New Field of Science, lecture, annual meeting of the American Physical Society, California Institute if Technology, www.zyvex.com/nanotech/feynman.html, July 13, 2006.

2. Drexler, K.E., "Engines of Creation", *Anchor Press*, New York, 1986.

3. Ding, B., Kim, H., Lee, S., Shao, C., Lee D., Park, S., et al., "Preparation and Characterization of a nanoscale poly(vinyl alcohol) fiber aggregate produced by an electrospining method", *Journal of Polymer Science: Part B: Polymer Physics,* 40, p1261, 2002.

4. Stephens, J., Frisk, S., Meglski, S., Rabolt, J., Chase, D., "Real time Raman studies of electrospun fibers", *Applied Spectroscopy*, 55, p1287, 2001.

5. Liu, H., Hsieh, Y., "Ultrafine fibrous cellulose membranes from electrospinning of cellulose acetate" *Journal of Polymer Science: Part B: Polymer Physics* 40, p2119, 2002.

6. Shin, Y., Hohman, M., Brenner, M., Rutledge, G., "Experimental characterization of electrospinning: the electrically forced jet and instabilities", *Polymer*, 42, p9955, 2001.

7. Schreuder-Gibson, H., Gibson, P., Senecal, K., Sennett, M., Walker, J., Yeomans, W., et al., "Protective textile materials based on electrospun nanofibers", *Journal of Advanced Materials*, 34(3), p44, 2002.

8. Fang, X., Reneker, D., "DNA fibers by electrospinning", *Journal of Macromolecule Science Physics,* B36, p169, 1997.

9. Matthews, J., Wnek, G., Simpson, D., Bowlin, G., "Electrospinning of Collagen Nanofibers", *Biomacromolecules,* 3, p232, 2002.

10. Kim, J., Lee, D., "Thermal properties of electrospun polyesters" *Polymer Journal*, 32, p616, 2000.

11. Shao, C., Kim, H., Gong, J., Lee, D., "A novel method for making silica nanofibres by using electrospun fibres of polyvinylalcohol/silica composite as precursor", *Nanotechnology*, 13, p635, 2002.

12. Dai, H., Gong, J., Kim, H., Lee, D., "A Novel Method for Preparing Ultra-Fine Alumina-Borate Oxide Fibres Via an Electrospinning Technique", *Nanotechnology*, 13, p674, 2002.

13. Choi, S., Chu, B., Lee, S., Lee, S., Im, S., Kim, S., Park, J., "Titania-doped Silica fibers Prepared by Electrospinning and Sol-Gel Process", 30, p215, 2004.

14. Viswanathamurthi, P., Bhattarai, N., Kim, H., Lee D., Kim, S., Morris, M., "Preparation and Morphology of Niobium Oxide Fibres by Electrospinning", *Chem. Phys. Lett.*, 374, p79, 2003.

15. Viswanathamurthi, P., Bhattarai, N., Kim, H., Khil, M., Lee, D., Suh, E., "GeO2 Fibers: Preparation, Morphology and Photoluminescence Property", *J. Chem. Phys.*, 121, p441, 2004.

16. Kim, H., Viswanathamurthi, P., Bhattarai, Lee, D., "Preparation and Morphology of Vanadium Oxide Fibers" *Chem. Phys. Lett.*, 5, p224, 2003.

17. Yang, X., Shao, C., Liu, Y., Mu R., Guan, H., "Nanofibers of CeO2 via an Electrospinning Technique", *Thin Solid Films*, 478, p228, 2005.

18. Yu, N., Shao, C., Liu, Y., Guan, H., Yang X., "Nanofibers of LiMn2O4 by electrospining", *J. Colloid Interface Sci.*, 285, p163, 2005.

19. Wang, Y., Santiago-Aviles, J., "Synthesis of Lead Zirconate Titanate Nanofibres and the Fourier-Transform Infrared Characterization of their Metallo-Organic Decomposition Process", *Nanotechnology*, 15, p32, 2004.

20. Park, H., “Fabrication of lanthanum copper oxide nanofibers by electrospinning,” Ph.D. Thesis, University of Florida, 2005.

21. Wu, Y., Hench, L., Du, J., Choy, K., Guo, J., ‘‘Preparation of Hydroxyapatite Fibers by Electrospinning Technique,’’ *J. Am. Ceram. Soc.*, 87, p988, 2004.

22. Madhugiri, S., Sun, B., Smirniotis, P., Ferraris, J., Balkus, K., “Electrospun Mesoporous Titanium Dioxide Fibers”, *Micropor.Mesopor.Mater.*,69, p77, 2004.

23. Dharmaraj, N., Park, H., Lee, B., Viswanathamurthi, P., Kim, H., Lee, D. “Preparation and Morphology of Magnesium Titanate Nanofibres Via Electrospinning”, *Inorg. Chem. Commun.*, 7, p431, 2004.

24. Dharmaraj, N., Park, H., Kim C., Kim H., Lee D., “Nickel Titanate Nanofibers by Electrospinning”, *Mater. Chem. Phys.*, 87, p5, 2004.

25. Wang, Y., Aponte, M., Leon, N., Ramos, I., Furlan, R., Evoy, S., Santiago-Aviles, J., “Synthesis and Characterization of Tin Oxide Microfibres Electrospun from a Simple Precursor Solution”, *Semicond. Sci. Technol.*, 19, p1057, 2004.

26. Yuh, J.,Nino, J., Sigmund, W., “Synthesis of Barium Titanate (BaTiO3) Nanofibers via Electrospinning”, *Mater. Lett.*, 59, p3645, 2005.

27. Guan, H., Shao C., Wen S., Chen, B., Gong, J., Yang, X., “A Novel Method for Preparing Co3O4 Nanofibers by Using Electrospun PVA/Cobalt Acetate Composite Fibers as Precursor”, *Mater. Chem. Phys.*, 82, p1002, 2003.

28. Shao C., Yang, X., Guan, H., Liu, Y., Gong, H., “Electrospun Nanofibers of NiO/ZnO Composite*”, Inorg. Chem. Commun.*, 7, p625, 2004.

29. Shao C., Yang, X., Guan, H., Liu, Y., Gong, H., Yu, N.,Yang, X., “A Novel Method for Making ZrO2 Nanofibres Via an Electrospinning Technique”, *J. Cryst. Growth,* 267, p380, 2004.

30. Li, D., Herricks, T., Xia, Y., “Magnetic Nanofibers of Nickel Ferrite Prepared by Electrospinning”, *Appl. Phys. Lett.*, 83, p4586, 2003.

31. Wang, A., Singh, H., Hatton, T., Rutledge, G., “Field-Responsive Superparamagnetic Composite Nanofibers by Electrospinning”, *Polymer*, 45, p5505, 2004.

32. Shao, C., Guan, H., Liu, Y., Li, X., Yang, X., Preparation of Mn2O3 and Mn3O4 Nanofibers via an Electrospinning Technique”, *J. Solid State Chem.*, 177, p2628, 2004.

33. Rayleigh, L., *Phil. Mag.* 14, p184, 1882.

34. Zeleny, J., *Phys. Rev.* 10, p1, 1917.

35. Vonnegut, B., Neubauer, R., “Production of monodisperse liquid particles by electrical atomization”, *Journal of Colloid Science*, 7, p616, 1952.

36. Taylor, G., “Electrically driven jets”, *Proceedings of the Royal Society of London*, 313, p453, 1969.

37. Hendricks, C., Hogan, J., Schneider, *AIAA Journal,* 2, p955, 1964.

38. Michelson, D., “Electrostatic atomization”, *Adam Hilger*, Bristol*,* 1990.

39. Hayati, I., Bailey, A., Tadros F., “Mechanism of stable jet formation in electrohydrodynamic atomization” *Nature* 319, p41, 1986.

40. Formhals, A., “Process and Apparatus for Preparing Artificial Threads”, *US Patent* 1975504, 1934.

41. Baumgarten, P., “Electrostatic spinning of Acrylic microfibers”, *J. Colloid Interface Sci.,* 36, p71, 1971.

42. Larrondo, L., Manley, R., “Electrostatic fibre spinning from polymer melts: Experimental observations on fibre formation and properties” *J. Polymer Sci.: Polymer Phys.,* 19, p909, 1981.

43. Larrondo, L., Manley, R., “Electrostatic fibre spinning from polymer melts: Examination of the flow field in an electrically driven jet” *J. Polymer Sci.: Polymer Phys.,* 19, p921, 1981.

44. Larrondo, L., Manley, R., “Electrostatic fibre spinning from polymer melts: Electrostatic deformation of a pendant drop of polymer melt” *J. Polymer Sci.: Polymer Phys.,* 19, p933, 1981.

45. Doshi, J., Reneker D., “Electrospinning process and applications of electrospun fibers”, *J. Electrostat.* 35, p151, 1995.

46. Fong, H. I.C., Reneker D. H., “Beaded nanofibers formed during electrospinning”, *Polymer*, 40, p4585, 1999.

47. Reneker D., Yarin, A., Fong, H., Koombhongse, S., “Bending instability of electrically charged liquid jets of polymer solutions in electrospinning”, *Journal of Applied Physics*, 87, p4531, 2000.

48. Fong, H., Reneker, D., “Electrospinning and the formation of nanofibers” *Hanser Gardner Publications*, NY, 2001.

49. Yarin, A. L., Koombhongse, S., Reneker, D., “Bending instability in electrospinning of nanofibers”, *Journal of Applied Physics 89*, p3018, 2001.

50. Doshi, J.,Reneker, D., “Electrospinning process and application of electrospun fibers”, *Journal of Electrostatics 35*, p151, 1995.

51. Hohman, M., Shin, M., Rutledge, G., Brenner, M., “Electrospinning and electrically forced jets. I. Stability theory”, *Physics of Fluids,* 13, p2201, 2001.

52. Hohman, M., Shin, M., Rutledge, G., Brenner, M., “Electrospinning and electrically forced jets: II. Applications” Physics of Fluids 13, p2221, 2001.

53. Shin, M., Hohman, M., Brenner, M., Rutledge, G., “Electrospinning: A whipping fluid jet generates submicron polymer fibers”, *Appl. Phys. Lett.* 78, p1149, 2001.

54. Deitzel, J., Kleinmeyer, J., Harris, D., Tan, N., “The effect of processing variables on the morphology of electrospun nanofibers and textiles” *Polymer* 42, p261, 2001.

55. Koombhongse, S., Reneker, D., “Branched and split fiber from electrospinning process”, *Book of Abstracts. In: New Frontiers in Fiber Science, Spring Meeting,* www.tx.ncsu.edu/jtatm/volume1specialissue/posters/posters_part1.pdf, February 2, 2006.

56. Pierre, A., “Introduction to sol-gel processing”, *Kluwer Academic Publishers*, 4, 1998.

57. Brinker, C., Scherer, W., “Sol-Gel Processing”, *Pergamon Press,* London, 1990.

58. Wright, J., Sommerdijk, N., “Sol-Gel Materials Chemistry and Applications”, *Taylor & Francis*, London, 2001.

59. Haertling, G., Land, C., *Ferroelectrics* 3, 269, 1979.

60. Yoldas, B., "Monolithic Glass Formation by Chemical Polymerization", *J. Mat. Sci.* 14, p1843, 1979.

61. Mouchon, E., Colomban, P., “Oxide ceramic matrix-oxide fibers woven fabric composites exhibiting dissipative fracture behavior”, *Composites* 26, p175, 1995.

62. Zhu, D., Jilavi, M., Kriven, W., “Synthesis and characterization of mullite and YAG fibers grown from deeply undercooled melts”, *Ceram. Eng. Sci. Proc.* 18, p31, 1997.

63. Chen, Y., Li, J., Dai J., 2001 “Si and SiOx nanostructures formed via thermal evaporation”, *Chemical Physics Letters,* 344, p450, 2001.

64. Liu, Z., Zhou, W., Sun, L., Tang, D., Zou, X., Li, Y., Wang, Y., Xie, S., “Growth of amorphous silicon nanowires”, *Chemical Physics Letters,* 341 p523, 2001.

65. Zhu, Y., Hu, W., Hsu, W., “A simple route to silicon-based nanostructures”, *Adv. Mater.* 11, p844, 1999.

66. Readey, M., “Formation and Sintering Characterization of Aluminum Borate Whiskers”, *J. Am. Ceram. Soc.* 75, p3452, 1992.

67. Liu, Y., Ren, W., Zhang, L., Yao, X., “New method for making porous SiO2 thin films”, *Thin Solid Films*, 353, p124, 1999.

68. Kern, W, et al., *Z. Phys.* 108, 295, 1938.

69. Nakane, K., Yamashita, T., Iwakura, K., Suzuki, F., “Properties and Structure of Poly(vinyl alcohol)/Silica Composites”, J. *Appl. Polym. Sci.* 74 p133, 1999.

70. Kern, W., “Infrared Spectroscopic Method for Compositional Determination of Vapor-Deposited Borosilicate Glass Films and Results of its Application”, *RCA Review,* 32, p429, 1993.

71. Matossi, F., *Z. Phys.* 108, p295, 1938.

72. Poh, N., Nur, H., Muhid M., Hamdan, H., “Sulfated AlMCM-41: Mesoporous Solid Bronsted Acid Catalysts for Dibenzoylation of Biphenyl”, *Catalysis Today*, 114, p257, 2006.

73. Andrianov, K., Bradley, D., “Metalorganic polymers” *Polymer Reviews*, New York, Interscience, vol 8, 1965.

74. Sopicka-Lizer, M., “Thermal Decomposition Of Aluminum Hydroxychloride” *Euroceramic,* Elsevier Appl. Sc, New York, vol 1, p1609, 1989.

75. Nishio, Y., Manley, R., “Cellulose-poly(vinyl alcohol) blends prepared from solutions in N,N-dimethylacetamide-lithium chloride”, *Macromolecules,* 21 p1270, 1988.

76. Hamzawy, E., Ali, A., “Sol-gel synthesis and crystallization of aluminum borosilicate”, Ceramics International, 27, p607, 2001.

77. Rainho, J., Rocha, J., Carlos, L., Almeida, R., “29Si Nuclear-Magnetic-Resonance and Vibrational Spectroscopy Studies of SiO2-TiO2 Powders Prepared by the Sol-Gel Process” J. Mater. Res. 16, p2369, 2001.

78. Xu, J., Thompson, S., O’Keefe, E., Perry, C., “Iron oxide-silica nanocomposites via sol-gel processing”, *Materials Letters* 58, p1696, 2004.

79. Koji, N., Tomonori, Y., Kenji, I., Fumio, S., *J. Appl. Polym. Sci.* 74, p133, 1999.

80. Chikako, N., Takeo, S., Toshio, Y., Masataka, S., “The effects of chromium compounds on PVA-coated AN and GAP binder pyrolysis, and PVA-coated AN/GAP propellant combustion”, *Fuel,* 77, p321, 1998.